iScience

CellPress
OPEN ACCESS

Article

An *In Vitro* Whole-Organ Liver Engineering for Testing of Genetic Therapies

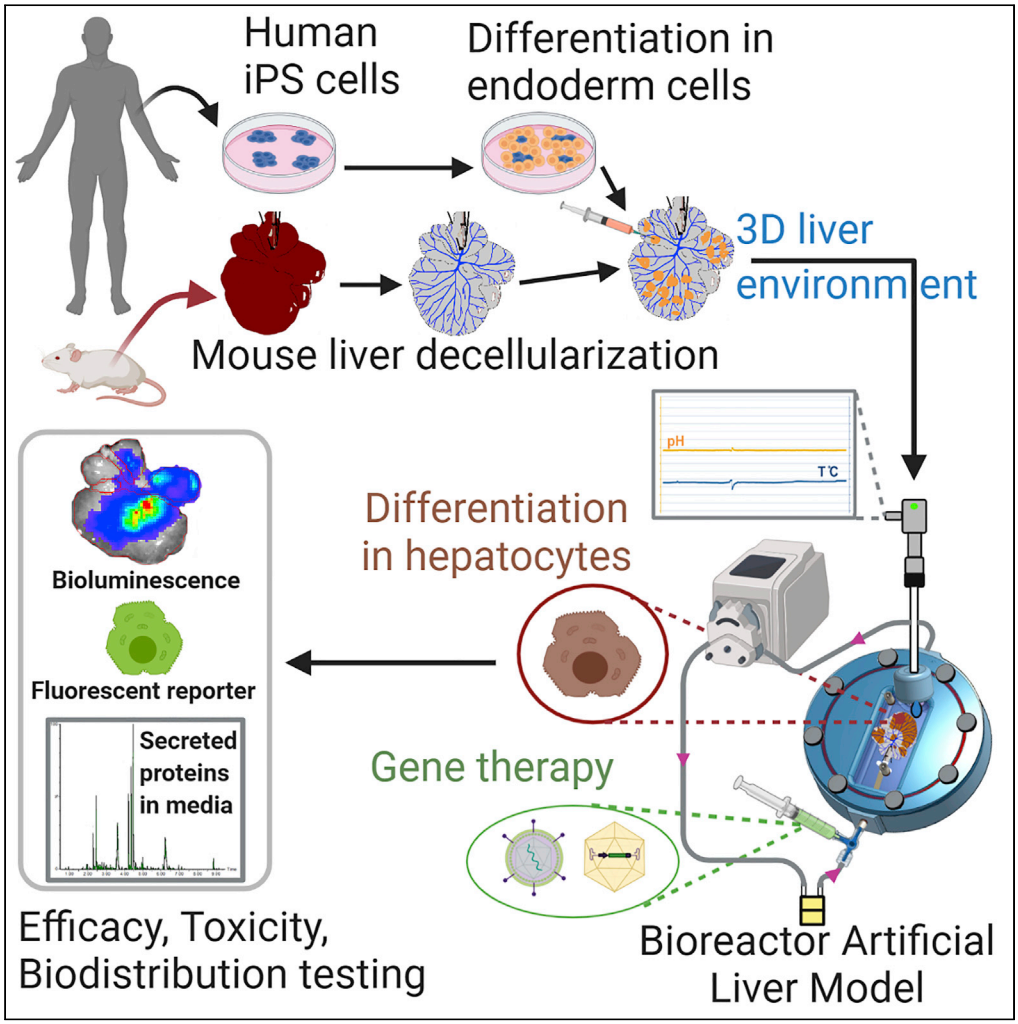

Maëlle Lorvellec, Alessandro Filippo Pellegata, Alice Maestri, ..., Tristan R. McKay, Paolo De Coppi, Paul Gissen

m.lorvellec@ucl.ac.uk

HIGHLIGHTS

Generation of a perfused humanized *in vitro* whole liver bioreactor model: BALM

BALM improves maturation and long-term survival of human iPS-derived hepatocytes

BALM allows viral transduction of human iHEPs through its vasculature

BALM provides a tool for gene therapy testing of human iHEPs

Lorvellec et al., iScience *23*, 101808
December 18, 2020
https://doi.org/10.1016/j.isci.2020.101808

iScience

CellPress
OPEN ACCESS

Article

An *In Vitro* Whole-Organ Liver Engineering for Testing of Genetic Therapies

Maëlle Lorvellec,[1,2,11,*] Alessandro Filippo Pellegata,[3] Alice Maestri,[1,2,9] Chiara Turchetta,[4] Elena Alvarez Mediavilla,[2] Soichi Shibuya,[3] Brendan Jones,[3] Federico Scottoni,[3] Dany P. Perocheau,[2] Andrei Claudiu Cozmescu,[1,5] Juliette M. Delhove,[6] Daniel Kysh,[1] Asllan Gjinovci,[1] John R. Counsell,[7] Wendy E. Heywood,[2] Kevin Mills,[2] Tristan R. McKay,[8] Paolo De Coppi,[3,10] and Paul Gissen[1,2,10]

SUMMARY

Explosion of gene therapy approaches for treating rare monogenic and common liver disorders created an urgent need for disease models able to replicate human liver cellular environment. Available models lack 3D liver structure or are unable to survive in long-term culture. We aimed to generate and test a 3D culture system that allows long-term maintenance of human liver cell characteristics.

The *in vitro* whole-organ "Bioreactor grown Artificial Liver Model" (BALM) employs a custom-designed bioreactor for long-term 3D culture of human induced pluripotent stem cells-derived hepatocyte-like cells (hiHEPs) in a mouse decellularized liver scaffold. Adeno-associated viral (AAV) and lentiviral (LV) vectors were introduced by intravascular injection.

Substantial AAV and LV transgene expression in the BALM-grown hiHEPs was detected. Measurement of secreted proteins in the media allowed non-invasive monitoring of the system.

We demonstrated that humanized whole-organ BALM is a valuable tool to generate pre-clinical data for investigational medicinal products.

INTRODUCTION

The liver accomplishes at least 500 vital functions ranging from bile production and protein synthesis to removal of blood toxins (Ehrlich et al., 2019). Liver transplantation is the only therapeutic option for a small proportion of monogenic liver-based disorders but is associated with significant morbidity and mortality, is limited by organ availability, and requires lifelong immune suppression. Treatments of liver diseases are complex, significantly impair patients' quality of life, and do not achieve perfect outcomes (Kriegermeier and Green, 2020; Martinelli et al., 2018).

Hence, liver-directed gene therapy, which consists of delivering a nucleic acid to compensate for a dysfunctional gene, is an attractive alternative (Baruteau et al., 2017). Different approaches that can be employed to modify endogenous genes include gene addition, gene editing, RNA-based therapies, and others. There has been a steady increase in liver-directed gene therapy clinical trials in recent years.

To ensure the success of gene therapy, the best delivery method and a vector that produces sufficient protein expression in target cells need to be selected (van Haasteren et al., 2018). Thus, the use of a model able to address these obstacles is essential.

Current *in vitro* liver models employ immortalized cell lines, like HepG2 or HepaRG, or primary human hepatocytes (PHHs) grown as a monolayer. These models, however, are of limited use owing to incomplete functional capacity (HepG2 and HepaRG cells), donor-to-donor variation, and rapid de-differentiation (PHHs). Two-dimensional (2D) cell cultures are grown at about 1% of normal tissues densities, which impairs intracellular signaling. To address these shortcomings three-dimensional (3D) *in vitro* models have been developed such as liver precision-cut tissue slices (PCTS), liver-on-a-chip microfluidic systems, and liver organoids. However, PCTS have only a short-term survival (Collins et al., 2019), whereas liver-on-chip

[1]MRC Laboratory for Molecular Cell Biology, University College London, London WC1E 6BT, UK

[2]Genetics and Genomic Medicine Department, Great Ormond Street Institute of Child Health, University College London, London WC1N 1EH, UK

[3]Developmental Biology and Cancer Research & Teaching Department, Stem Cells & Regenerative Medicine Section, Great Ormond Street Institute of Child Health, University College London, London WC1N 1EH, UK

[4]Department of Chemistry, Materials and Chemical Engineering "Giulio Natta," Politecnico di Milano, Milan 20133, Italy

[5]NIHR Great Ormond Street Hospital Biomedical Research Centre, University College London, London WC1N 1EH, UK

[6]Robinson Research Institute, University of Adelaide, Adelaide, SA, 5006, Australia

[7]Dubowitz Neuromuscular Centre, Molecular Neurosciences Section, Developmental Neurosciences Programme, UCL Great Ormond Street Institute of Child Health, London WC1N 1EH, UK

[8]Centre for Bioscience, Manchester Metropolitan University, Manchester M1 5GD, UK

[9]Present address: Cardiovascular Medicine Unit, Department of Medicine, Center for Molecular Medicine, Karolinska Institutet, Stockholm 171 76, Sweden

Continued

microfluidic systems and organoids do not reflect the 3D liver architecture and lack natural extracellular matrix (ECM) and vascularization, essential for nutrient and oxygen exchange (Akbari et al., 2019).

Rodent disease models offer many advantages over *in vitro* liver models; however, the physiological and genomic interspecies differences pose limitations in the representation of the disease phenotypes (Mariotti et al., 2018; Martignoni et al., 2006) and vector targeting. Recombinant AAV8 vector was used in the first successful gene therapy clinical trial, which targeted hepatocytes (Nathwani et al., 2014). A small increase (achieving <10% of normal) in the plasma circulating factor IX, secreted by the liver, was sufficient to improve patients' phenotype. Much higher FIX levels were seen in the preclinical studies likely owing to the differences in hepatocyte transduction by AAV8 between humans and mice (Manno et al., 2006; Lisowski et al., 2014). Humanized FRG mice (where mouse liver is partially repopulated by human hepatocytes) is a better model to study human hepatocyte vector transduction (Strom et al., 2010); however, they are extremely resource intensive and require patient-specific hepatocytes in order to demonstrate disease phenotype.

Here we demonstrate testing of viral gene therapy vectors in an *in vitro* whole-organ "Bioreactor grown Artificial Liver Model" (BALM) that employs bioreactor for long-term 3D culture of human induced pluripotent stem cells (hiPSCs)-derived hepatocyte-like cells (hiHEPs). hiPSCs can provide an unlimited source of patient-derived cells, which can be differentiated toward hepatocyte lineage. BALM uses mouse decellularized liver scaffolds as growth support, with a preserved extracellular matrix (ECM) and 3D structure previously shown to promote a faster maturation of hiHEPs (Lorvellec et al., 2017).

Bioreactor provides controlled and dynamic culture conditions and is the solution to the development of 3D organ models. The concept of using bioreactor-engineered whole-organ systems could overcome some of the current caveats of *in vitro* and *in vivo* modeling and improves the chance of more accurate preclinical therapy testing outcomes.

RESULTS

Generation of BALM

The mouse livers were decellularized via cannulation of the portal vein (PV) by detergent-enzymatic treatment (DET), which preserves the natural ECM and the vascular network (Maghsoudlou et al., 2016; Mazza et al., 2017) (Figure S1). The hiPSCs line previously used to generate hiHEPs (Song et al., 2009; Yusa et al., 2011) was differentiated toward definitive endoderm-like cells (DECs). DECs harvested at day 6 of differentiation were injected into multiple locations of the parenchyma of individual lobes of the mouse decellularized liver scaffolds. DEC differentiation toward hepatocytes was then continued in the bioreactor with the hepatic specification stage from day 7 to day 11 followed by the hepatic maturation stages 1 and 2 (Figure 1A). The stage-specific media, 3D environment, and liver ECM of the scaffold were previously shown to promote faster maturation of hiHEPs (Lorvellec et al., 2017).

The seeded decellularized livers were placed into the chamber of the bioreactor and connected to the circuit via its catheter at the entrance of the chamber. The volume of the chamber is 50.2 cm^3 keeping the media to a minimum volume of 20 mL. Media circulation in a closed circuit was driven by a roller pump, which delivered flow perfusion through the vascular network. This system permits nutrients and oxygen to reach the whole scaffold and creates dynamic shear stress, important for orientation of polarized epithelial cells such as hepatocytes (Tharp and Weaver, 2018; You et al., 2019; Dash et al., 2013). Media changes and collection were facilitated by the three-way connector at the exit of the chamber. A bubble trap before the entrance of the chamber eliminated air bubbles to avoid embolization of the scaffold. The media was oxygenated using a 5% CO_2/Air gas cylinder regulated by a flowmeter, and the gas was humidified in a water bottle, avoiding excess evaporation while an overflow bottle collected outflow humidity. The system was maintained at 37°C using a hot plate placed under the chamber and the two bottles. The temperature and pH were monitored in real time by using a sterile dip sensor. The transparent lid of the chamber allowed visual monitoring of the scaffold (Figures 1B and 1C). A three-way connector placed before the entrance of the chamber permitted the perfusion of compounds or gene therapy products. The bioreactor system provides a sterile and controlled environment for the culture of the 3D whole-organ system. No malfunctioning or contaminations occurred during the experiments. The pH monitoring reported maintenance of the culture in the range of 7–7.8 with fluctuation derived from media changes according to the protocol (Figure 1D). BALM was maintained until day 27 of cell differentiation.

[10]Senior Authors

[11]Lead Contact

*Correspondence: m.lorvellec@ucl.ac.uk

https://doi.org/10.1016/j.isci.2020.101808

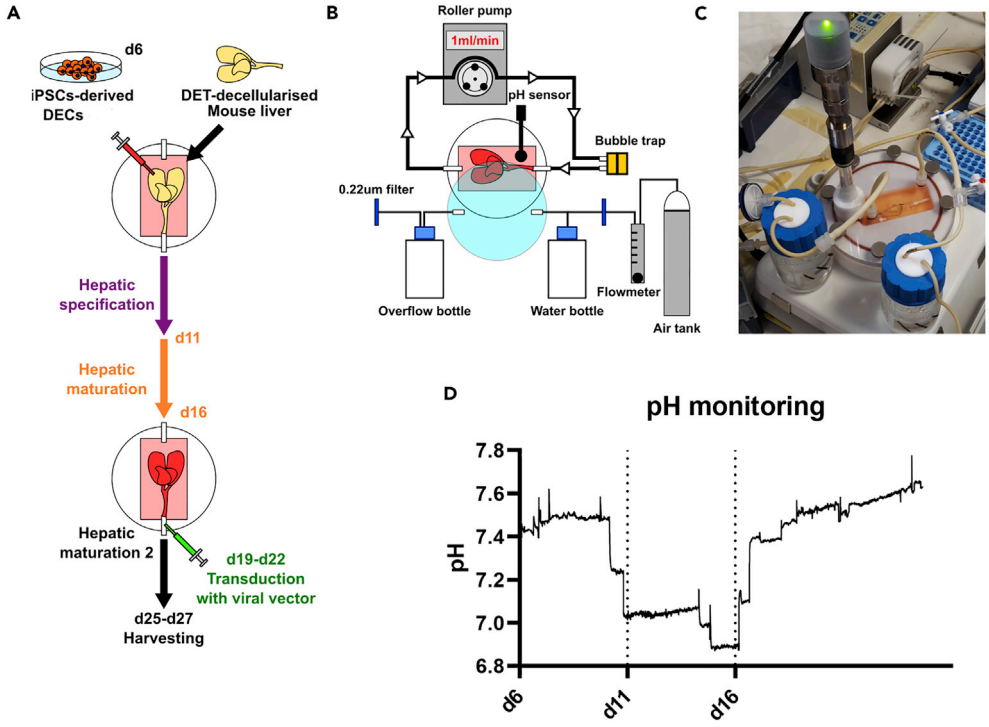

Figure 1. BALM Generation

(A) hiPSCs differentiated to DECs, mouse livers decellularized using DET method. DECs injected into multiple locations in individual lobes on day 6 of differentiation. Then livers were placed into bioreactor and cultured under perfusion. Hepatic specification stage: day 7 to day 11 followed by hepatic maturation. During the maturation stage, viral vectors were perfused through the vasculature. BALMs were kept in culture till day 27.

(B) Stand-alone bioreactor composed of a chamber with medium in a closed circuit with a roller pump. The medium is oxygenated by 5% CO_2/Air gas cylinder regulated by a flowmeter. The gas is humidified in a water bottle while an overflow bottle collects outflow humidity. A bubble trap before the entrance of the chamber eliminates air bubbles. The system is maintained at 37°C using a hot plate under the chamber and the bottles.

(C) Bioreactor macroscopic appearance.

(D) Representative graph of pH monitoring of BALM, black dotted bars mark media type changes, values are average of two experiments.

See also Figure S1.

BALM Allows Repopulation by hiHEPs Expressing Mature Hepatocyte Markers and Coculture with Endothelial Cells

The mouse decellularized liver scaffolds generated by DET were visually evaluated for the quality of vascular perfusion by injection of colored media via the PV catheter. After seeding, injection sites were observed in each seeded lobe as opaque masses among transparent surrounding tissue. After 25 days of differentiation in BALMs, the whole tissue became opaque (Figure 2A).

DAPI and H&E staining of cryosections of the individually seeded liver lobes showed many cell nuclei, whereas in the control unseeded lobes only the ECM fibers were visible (Figures 2B and 2C). hiPSC-derived cells successfully repopulated the scaffolds and appeared to be positioned along the scaffold fibers. We previously demonstrated that the amount of DNA left in the decellularized liver is negligible compared with the fresh liver tissue (0.093 and 1.068 μg/mg, respectively) (Lorvellec et al., 2017). Ki-67, a marker of proliferation was highly expressed at day 21 of differentiation, whereas there were only a few apoptotic cells as shown by cleaved caspase-3 immunofluorescence staining. Cell viability assay showed mitotically active cells in BALMs at days 20, 26, and 27 (Figures 2D, S2, and S5).

Expression of characteristic hepatocyte markers was analyzed on days 25–27 of differentiation in BALMs. Immunofluorescence staining of cryosections of seeded lobes showed that a high number of cultured hi-HEPs expressed albumin (ALB), a mature cytoplasmic hepatocyte marker, whereas few cells expressed

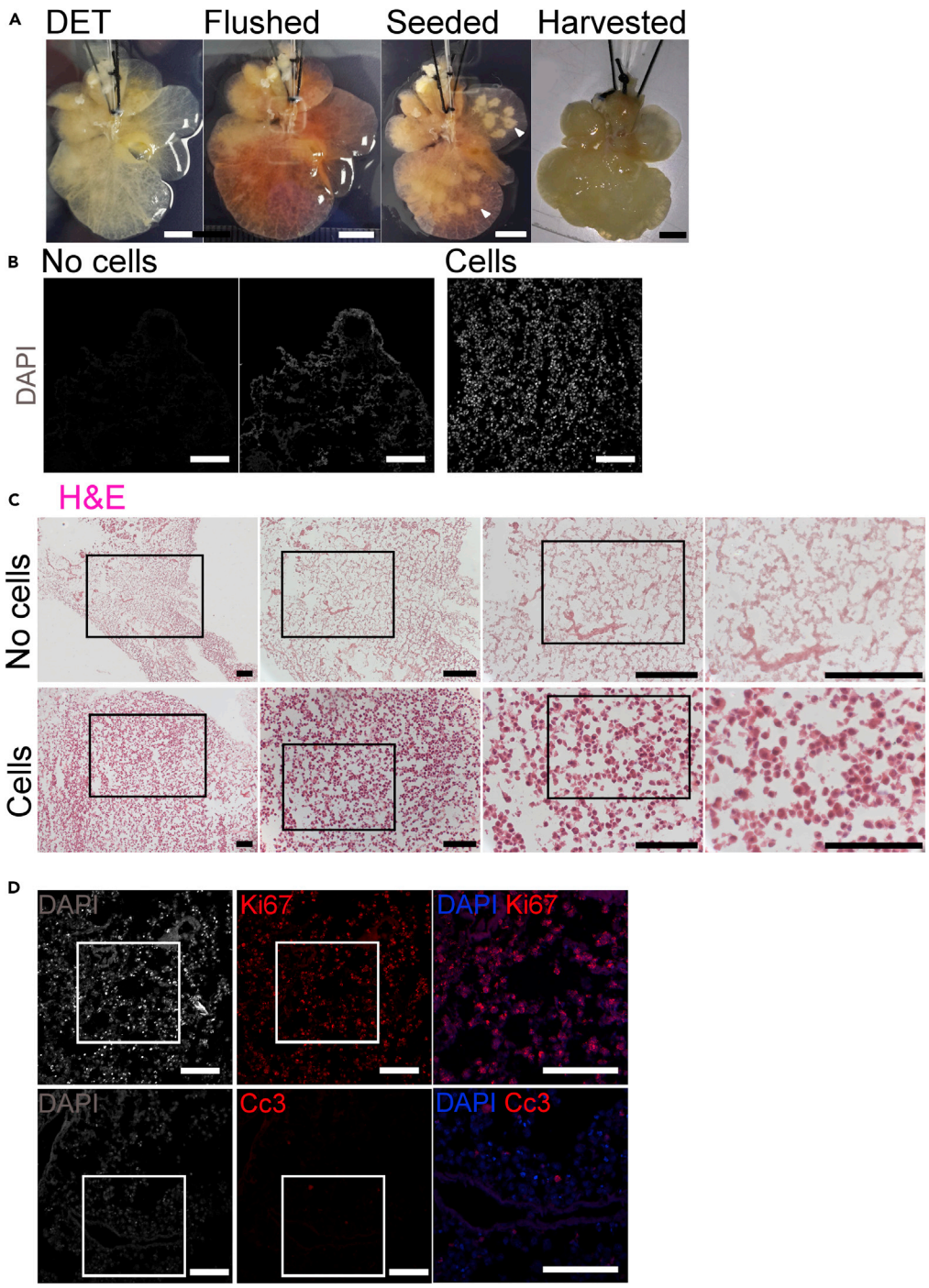

Figure 2. BALM Cell Repopulation

(A) Macroscopic appearance of a mouse liver scaffold during seeding and culture. Decellularized liver is flushed with media to identify well-perfused lobes, which are seeded on day 6; the white arrows indicate the visible pockets of DECs. Scaffold harvested at day 25 of differentiation loses transparency. Scale bar, 5 mm.

(B) DAPI nuclear staining (grey) show ECM fibres and absence of nuclei on a cryosection of an unseeded lobe (middle and left). hiPSCs-derived nuclei are present along scaffold fibres of a cryosection of a DECs seeded lobe at day 26 (right). DAPI intensity gains are identical between left and right image, middle image is intensity gain x4 of left image to visualize the ECM fibres. Scale bar 100 μm. (C) H&E staining (nuclei stained in purple and ECM in pink) also show ECM fibres and absence of cells on a cryosection of an unseeded lobe (top). hiPSCs-derived cells appear to be positioned along the

Figure 2. *Continued*
scaffold fibres of a cryosection of a DECs seeded lobe at day 26 (bottom). Higher magnification images correspond to the delineated lower magnification images in the adjacent panel. Scale bar 100 μm.
(D) Ki-67 staining of a cryosection of a DECs seeded lobe at day 21 shows proliferating cells (top) and few apoptotic cells as shown by Cc3-positive staining (bottom). Nuclei stained with DAPI. Scale bar, 100 μm.
See also Figures S2 and S5 and Table S3.

alpha-fetoprotein (AFP), a fetal cytoplasmic hepatocyte marker. A high number of cells also expressed the intermediate filament protein cytokeratin 18 (CK-18) but none cytokeratin 19 (CK-19) or cytokeratin 7 (CK-7) (data not shown). Although CK-18-and CK-19 are both expressed at the hepatoblast stage of hepatocyte differentiation, in mature cells, CK-18 marks hepatocytes, whereas CK-19, similarly to CK-7 expression, is specific to cholangiocytes (Chougule and Sumitran-Holgersson, 2012; Xu et al., 2007). Interestingly, asialoglycoprotein receptor (ASGPR), which is normally localized at the sinusoidal membrane of the mature hepatocytes, was restricted to a part of the membrane in cells cultured in BALMs. Thus, taken together, these findings suggest cell differentiation toward mature hepatocytes (Figures 3A, S3, and S5).

Synthesis of plasma proteins is one of the hepatocyte functions with ALB being the most abundant. ALB production increases as hepatocytes mature from fetal to the adult cell type. AFP expression, on the contrary, is high in the fetus but drops soon after birth (Elmaouhoub et al., 2007; Nayak and Mital, 1977).

To monitor in a non-invasive manner the secretion of hepatic proteins, we harvested the BALM media during the hepatocyte maturation stage 2 and used targeted proteomic liquid chromatography with tandem mass spectrometry (UPLC-LC/MS/MS) technique to measure tryptic peptides from ALB and AFP. As the number of cells alive at the time of measurement is unknown, we calculated the ratio ALB/AFP. We observed that the ALB/AFP ratio increases from d19 of differentiation till d25, with raw data suggesting that this is the result of overall increase in ALB and decrease in AFP (Figure 3B and Table S1). In concordance with the microscopy results, the increased ratio would also point toward hiHEPs becoming more mature during BALM culture.

To investigate whether endothelial cells could repopulate BALM vasculature and whether BALM could sustain coculture of different cell types, we perfused human umbilical vein endothelial cells (HUVECs) through the PV catheter and cocultured them with DECs up to day 21 of differentiation. Immunofluorescence staining of cryosections of DECs seeded lobes showed that only cells in the vasculature expressed CD31, an endothelial marker. HUVECs were able to repopulate BALM's vasculature network and were still proliferating as well as hiHEPs (Figures 3C, S3, and S5). We did not observe any detrimental effects of the HUVECS on hiHEPs differentiation.

BALM as a Tool to Evaluate Viral Vector-Based Gene Therapy

AAV and lentiviruses (LVs) are the most commonly used viral gene therapy vectors. A number of clinical trials are in progress using *in vivo* administered AAVs targeting liver cells. Although so far LVs have been used only for *in vitro* gene therapy applications, there are potential advantages of these vectors for *in vivo* use such as efficient human hepatocyte transduction and genomic integration leading to stable gene expression in growing liver (van Haasteren et al., 2018; Zabaleta et al., 2019; Catapult, 2020).

We investigated whether BALM can be used to test the efficiency of AAV and LV vectors for human liver cell transduction. Both types of vectors were perfused through the vasculature, during the maturation stage 2 (Figure 1A).

For the AAV experiment, we selected rAAV-LK03 previously shown to preferentially transduce primary human hepatocytes *in vitro* and *in vivo* (Lisowski et al., 2014; Paulk et al., 2018). The rAAV-LK03-CMV-eGFP vector drives eGFP expression under the control of the ubiquitous cytomegalovirus (CMV) promoter (Figure 4A). BALMs were perfused at day 21 of differentiation with rAAV-LK03-CMV-eGFP for 96 h (day 25 of differentiation) then replaced with fresh media and harvested at day 27 of differentiation. Immunofluorescence staining of eGFP performed on cryosections of individual lobes showed GFP-positive cells in BALMs transduced for 4 days with rAAV-LK03-CMV-eGFP (Figures 4D and S5) thus demonstrating successful transduction of hiHEPs.

For the LV experiment, we selected an LNT-LXR-Nluc/eGFP, which carries a hepatic transcription factor activated reporter construct (Buckley et al., 2015; Delhove et al., 2017) made of Liver X Receptor (LXR) response elements upstream of the adenoviral E1A minimal promoter sequence driving both the

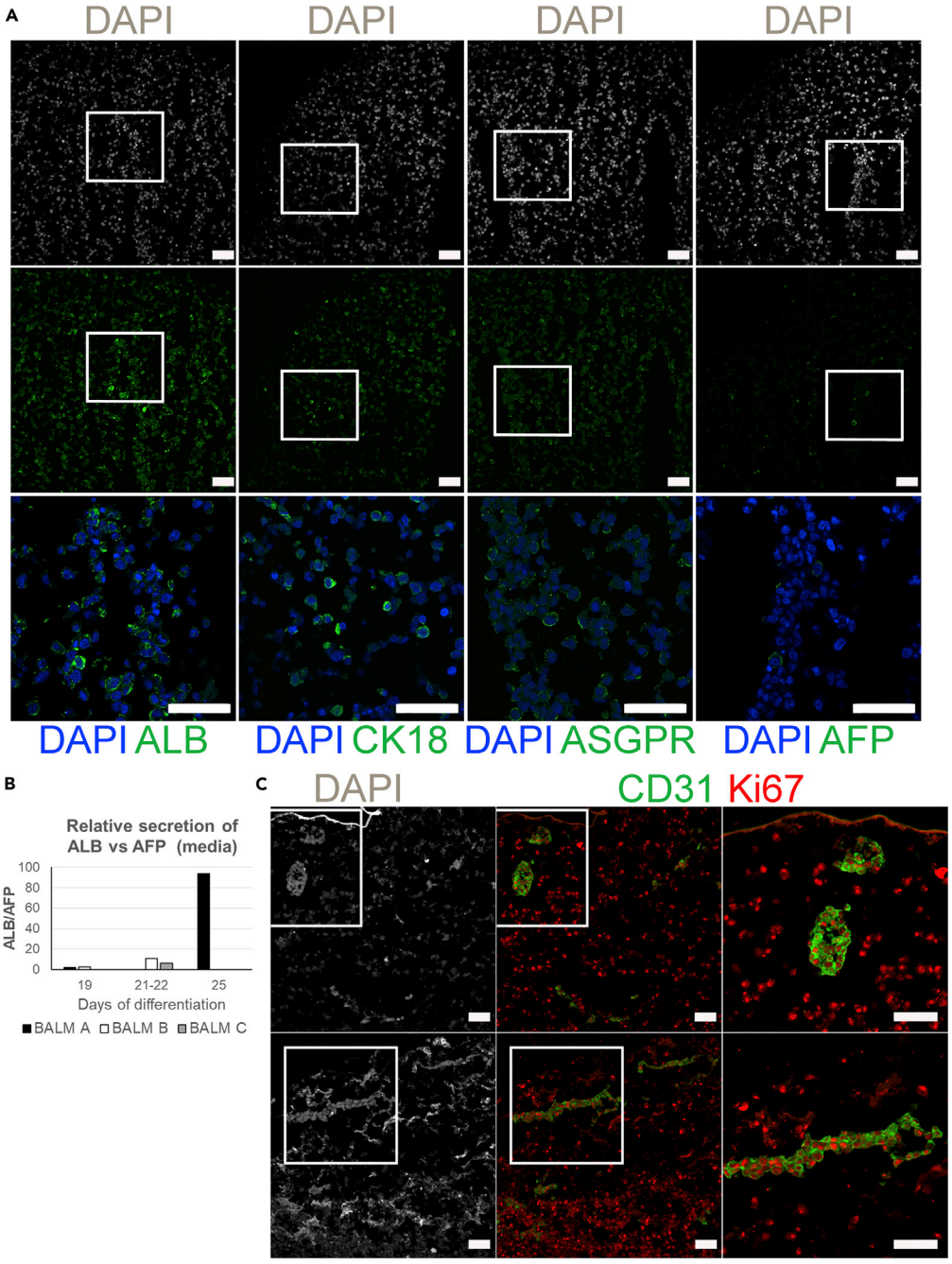

Figure 3. hiHEPs and HUVECs in BALM

(A) Hepatocyte markers expression by hiHEPs in BALM on day 26 of differentiation. Widespread ALB and CK-18 expression with minimal AFP expression. Higher magnification images of merged channels in the bottom panel correspond to the delineated lower magnification images. Hepatocyte sinusoidal membrane protein ASGPR is localized at the cell membrane. Nuclei stained with DAPI. Scale bar, 50 μm.

(B) ALB and AFP secretion as detected by UPLC-LC/MS/MS. Three BALMs at different days of differentiation.

(C) Immunostaining of CD31 and Ki-67 shows HUVECs repopulation of the vasculature; proliferating hiHEPs and HUVECs on day 21 of differentiation. Higher-magnification images of merged channels in the right panel correspond to the delineated lower-magnification images. Nuclei stained with DAPI. Scale bar, 50 μm.

See also Figures S3 and S5 and Tables S1, S3, and S4.

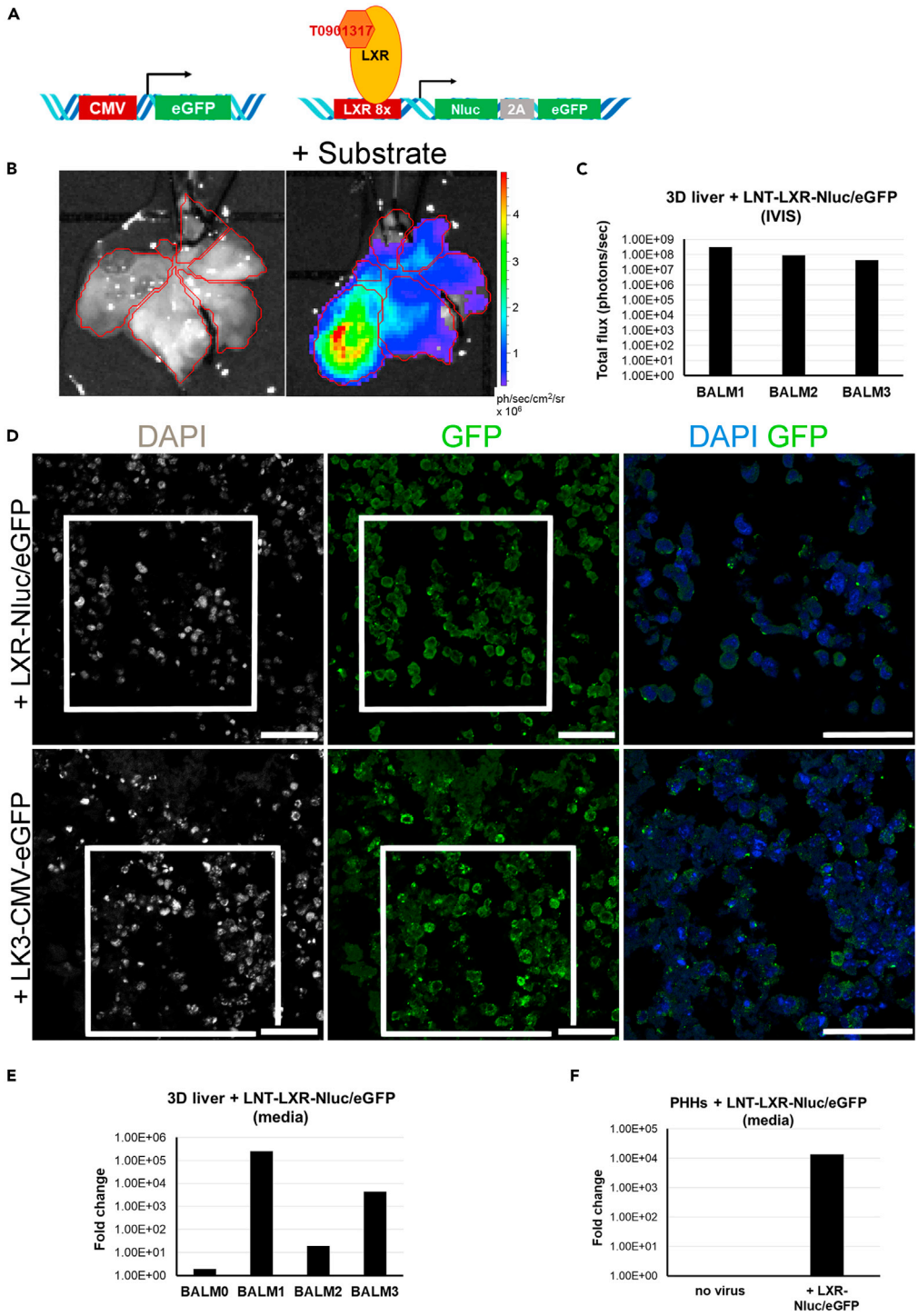

Figure 4. LV and AAV Testing in BALMs

(A) AAV and LV vectors. rAAV-LK03-CMV-eGFP (left) and LNT-LXR-Nluc/eGFP and LXR with its agonist T0901317 (right).
(B) Bioluminescence imaging of BALM1 transduced with LNT-LXR-Nluc/eGFP and agonist activation show luciferase expression after PV perfusion with a luciferase substrate in the DECs seeded lobes at day 25 (1 min exposure).
(C) Bioluminescence quantification of BALM1-3 after luciferase substrate perfusion (1 min exposure) at day 25.
(D) Immunostaining of GFP shows positive hiHEPs when transduced with LNT-LXR-Nluc/eGFP (BALM2, top panel) or with rAAV-LK3-CMV-eGFP (BALM4, bottom panel). Higher magnification images of merged channels in the right panel correspond to the delineated lower magnification images. Nuclei stained with DAPI. Scale bar, 50 μm.

Figure 4. *Continued*
(E) Bioluminescence fold change of secreted nanoluciferase in the media of BALM1-3 shows luciferase secretion upon LXR induction by its agonist at days 25–26. Untransduced negative control BALM (BALM0).
(F) Bioluminescence fold change of secreted nanoluciferase in the media of PHHs transduced with LNT-LXR-Nluc/eGFP for 24 h followed by 48 h incubation with 1 μM agonist shows luciferase secretion in PHHs.
See also Figures S4 and S5 and Tables S2 and S3.

expression of eGFP fluorescence and secreted NanoLuc luciferase (Nluc) for live imaging, immunofluorescence staining, and luciferase assay of the culture media. LXRα is highly expressed in hepatocytes and regulates expression of genes important for various hepatocyte functions (Ma and Nelson, 2019; Komati et al., 2017; Maqdasy et al., 2016; Chen et al., 2014). This reporter construct allows monitoring of cell viability and their response to LXR agonist in real time without cell lysis. The synthetic agonist T0901317 used in this study has been shown to upregulate LXR (Komati et al., 2017; Mitro et al., 2007) (Figure 4A). The optimal concentration of 1 μM agonist was determined using hiHEPs in 2D culture (Figure S4).

BALMs were perfused on day 19 for 48 h with LNT-LXR-Nluc/eGFP, then fresh media with 1 μM T0901317 agonist was added on day 21 for 96 h (till day 25 of differentiation). The NanoLuc luciferase reagent furimazine was administered by perfusion through the catheter (Nano-Glo Luciferase assay, Promega). Live bioluminescence was observed before and after addition of the substrate showing activation of the LNT-LXR-Nluc/eGFP reporter construct inside the seeded lobes of the scaffold with average RLU/scaffold ranging from 4×10^7 to 3.3×10^8 ph/s (Figures 4B and 4C and Table S2). Immunofluorescence staining of eGFP was performed on cryosections of individual lobes and showed GFP-positive cells in BALMs transduced for 2 days with LNT-LXR-Nluc/eGFP (Figures 4D and S5).

The small NanoLuc luciferase is secreted into the media and therefore allows monitoring of luciferase activity by simply sampling the media from the bioreactor. Initially, PHHs were transduced for 24 h in 2D culture. Then fresh media with 1 μM T0901317 agonist was added for 48 h and the media was assayed for luciferase activity; 3.08×10^5 PHHs gave a fold change of 1.3×10^4 (Figures 4F and Table S2).

Media were collected from BALMs on day 19 before transduction (d19-d21) and on day 25 after activation (d21-d25). Luciferase assay of the media collected showed an increase fold change from day 19 to day 25 in all three transduced BALMs with LNT-LXR-Nluc/eGFP (BALM 1–3: 1.92×10^1-2.51×10^5) compared with a non-transduced BALM (BALM 0: 1.89) (Figures 4E and Table S2).

Thus, we showed that LV could transduce hiHEPs when delivered through the vasculature of the whole-organ liver model. Bioluminescence imaging performed on the day of harvest demonstrated that the cells were alive at that time and the LXR receptor was active in those cells. Furthermore, it also allowed us to locate the highest density of live cells within the scaffold.

DISCUSSION

Cell culture models are fundamental instruments for basic and translational research. Clinical trials frequently fail owing to the lack of direct translation from preclinical experiments into human studies (Manno et al., 2006; Pound and Ritskes-Hoitinga, 2018). The development of models that can better replicate human tissue complexity is needed.

The BALM system has several advantages over conventional *in vitro* models. It utilizes hiHEPs, which, once derived from disease-specific hiPSCs, could allow disease modeling and phenotype correction. The scaffolds derived from adult mice livers provide the ECM proteins and the 3D structure reproducing the *in vivo* liver environment and can be obtained from repurposed animals, and therefore, this approach is aligned with the 3Rs (replacement, reduction, and refinement) of animal research. The stand-alone bioreactor is independent of a cell culture incubator, allowing the device to be located on a standard laboratory benchtop. Different parameters can be easily adjusted in this controlled environment such as oxygen level, moving from normoxia to hypoxia; temperature; and pH, which can be monitored in real time. The latter is essential as it influences cell proliferation and cell volume; pH of the media below 6.8 or above 8 is detrimental to cell growth (Mackenzie et al., 1961). Furthermore, tight control of intracellular pH of hepatocytes is essential for its metabolic roles, including urea synthesis, glycolysis, and bile electrolyte secretion (Pollock, 1984; Strazzabosco and Boyer, 1996; Park et al., 1979).

The cannulation of the portal vein (PV) in our model allows delivery of oxygen, nutrients, and therapeutic products through the liver vasculature mimicking the natural conditions. Indeed the liver receives 25% of the cardiac output, mostly via the portal vein (van Haasteren et al., 2018). The advantage of having PV access allows modification of the flow in the vascular network using the roller pump controlling the fluid shear stress (Tresoldi et al., 2015). Moreover, we demonstrated that AAV and LV vectors can transduce the hiHEPs in BALM when delivered via the PV and can drive transgene expression. BALMs can also be used to investigate repeated delivery of therapeutics.

In contrast to BALM, most *in vitro* models including organoids and liver-on-chip microfluidic systems lack the extensive vasculature or sinusoids that are needed for nutrient exchange. The small dimensions of the microfluidic systems allow surface effects to dominate volume effects leading to a laminar flow with little mixing (Cavero et al., 2019), which does not fully represent the mechanical forces within the liver. Although some new micro-fluidic 3D models allow co-culture of different liver cells (Vernetti et al., 2016), the natural liver-derived scaffolds are a better biological material for absorption of nutrients than the artificial fabric (Ehrlich et al., 2019) as it provides the natural 3D architecture and tissue-specific signaling, which has a role in the regulation of liver cell function (Sellaro et al., 2010; You et al., 2019), migration, and proliferation (Uygun et al., 2010).

The development of functional assays using bioreactor media as well as the use of bioluminescent or fluorescent reporters allow non-invasive monitoring of cell viability and function. The BALM cultured hiHEPs were alive and functional on day 27 of differentiation evidenced by secreted ALB and AFP detection as well as the LXR reporter activity. The differentiation of hiPSC and the prolonged culture in the bioreactor allowed the delivery of the gene therapy products at different stages of human hepatocyte development and permitted its long-term study.

To improve BALMs, the number of DECs seeded on day 6 could be scaled up enhancing the overall distribution of the hepatocytes throughout the scaffold. Higher cell numbers would improve the development of the functional assays as most routinely used 2D assays have to be adapted to the challenges of the BALM system where the cells are less easily accessible to examination and their secreted products are highly diluted in the bioreactor media. Development of bioreactor-specific assays to study ureagenesis or gluconeogenesis would be highly beneficial to further characterize the functionality of hiHEPs.

Further improvements could benefit BALMs. Although coculture of hiHEPs and HUVECs seeded through the PV allowed a better mimicking of the liver environment (Huang et al., 2020), it has been very recently shown that also endothelial and biliary cell types could be derived from human iPSC and co-seeded with iPSC-derived hepatocytes in decellularized livers to form functional mini livers. The latter could be used for auxiliary transplantation in immunocompromised rats and remain functional for 4 days *in vivo* (Takeishi et al., 2020). Moreover, multiple cannulations of hepatic artery, hepatic veins, and bile duct would provide additional delivery routes for other liver cells and therapeutic compounds. This will require a combination of culture media that would allow co-culture of all liver cells (Ehrlich et al., 2019), but it may help to establish the metabolic zonation (Ehrlich et al., 2019), which would make this 3D whole organ even more representative of live conditions and facilitate testing of drug delivery to the whole-cell gamut.

In conclusion, the humanized whole-organ liver model BALM is a valuable tool that could replace some of the *in vitro* and *in vivo* therapeutic testing approaches generating high-value pre-clinical data.

Limitations of the Study

BALM has a few challenges to overcome linked to its 3D nature: it contains a small proportion of cells, not easily accessible, for a high amount of ECM, and their secreted products are highly diluted in the bioreactor media. Establishing a standard curve for cell viability assays was impaired owing to lack of cells with similar metabolism to the hiHEPs differentiated in BALMs and to 2D versus 3D differences: reagent's incubation time and dilution, percentage of hiHEPs and background level. Nevertheless, the presto blue assay could be used to show a relative effect of a particular condition between two lobes but not to determine the exact number of viable cells within each lobe. The unknown number of alive cells within BALM and the difficulty to standardize how much proteins is produced by the cells at a certain time point means that instead of an accurate amount of protein produced by BALM, we have to express protein expression as a ratio like ALB/AFP using UPLC-LC/MS/MS. Furthermore, the difficulty to extract alive cells from BALM means techniques such as single-cell RNA sequencing are not directly applicable and requires further development.

Resource Availability

Lead Contact

Further information and requests for resources and reagents should be directed to and will be fulfilled by the Lead Contact, m.lorvellec@ucl.ac.uk.

Materials Availability

This study did not generate new unique reagents.

Data and Code Availability

This study did not generate datasets/code.

METHODS

All methods can be found in the accompanying Transparent Methods supplemental file.

SUPPLEMENTAL INFORMATION

Supplemental Information can be found online at https://doi.org/10.1016/j.isci.2020.101808.

ACKNOWLEDGMENTS

This research was supported by the European Research Council (EU) grant ERC-2013-StG-337057 (to P.G.) and by the Medical Research Council (UK) Confidence in Concept scheme awarded to the University College London, MC_PC_18063 (UK). P.D.C. is supported by the National Institute for Health Research (NIHR) and W.E.H. is supported by the NIHR Great Ormond Street Hospital Biomedical Research Center (NIHR GOSH BRC).S.S. is subsidised by the Japan society for the promotion of science overseas research fellowships, 310072 (JP) and B.J. by General Sir John Monash Foundation, Eric Bishop Research Scholarship, Royal Australasian College of Surgeons (AU) and UCL Overseas and Graduate Research Scholarships (UK). J.M.D. was funded by the European Research Council (EU) grant "Somabio" 260862 and the National Centre for the Replacement, Refinement and Reduction of Animals in Research, NC/L001780/1 (UK). J.R.C. is funded by a Wellcome Innovator Award, 210774/2/18/Z (UK). T.R.M. is funded by European Union Horizon 2020 project BATCure, 666918 (EU). This work was supported by Medical Research Council (MRC) core funding to the MRC Laboratory for Molecular Cell Biology at University College London, MC_U12266B. All research at Great Ormond Street Hospital National Health Service (NHS) Foundation Trust and UCL Great Ormond Street Institute of Child Health is made possible by the NIHR GOSH BRC (UK). The views expressed are those of the author(s) and not necessarily those of the NHS, the NIHR, or the Department of Health.

We thank Prof. Ludovic Vallier (Cambridge University, UK) for providing the hiPSCs line and Dr Leszek Lisowski (University of Sidney, AU) for providing the rAAV-LK03 CMV-eGFP viruses.

The graphical abstract was created with BioRender.com.

AUTHOR CONTRIBUTIONS

Conceptualization, M.L., A.F.P., P.D.C., and P.G.; Methodology, M.L., A.F.P., W.E.H., and K.M; Investigation, M.L., A.F.P., A.M., C.T., E.A.M., S.S., B.J., F.S., D.P.P., D.K., and A.G.; Formal Analysis, M.L. and E.A.M.; Visualization, M.L. and A.F.P.; Resources, C.C., J.R.C., J.M.D., and T.R.M.; Supervision, P.D.C. and P.G.; Funding Acquisition, P.G.; Writing – Original Draft, M.L., A.F.P., and P.G.; Writing – Review & Editing, M.L., A.F.P., and P.G. with input from all authors.

DECLARATION OF INTERESTS

The authors declare no competing interests.

Received: July 7, 2020
Revised: October 19, 2020
Accepted: November 10, 2020
Published: December 18, 2020

REFERENCES

Akbari, S., Arslan, N., Senturk, S., and Erdal, E. (2019). Next-Generation liver medicine using organoid models. Front. Cell Dev. Biol. *7*, 345.

Baruteau, J./., Waddington, S.N., Alexander, I.E., and Gissen, P. (2017). Gene therapy for monogenic liver diseases: clinical successes, current challenges and future prospects. J. Inherit. Metab. Dis. *40*, 497–517.

Buckley, S.M., Delhove, J.M., Perocheau, D.P., Karda, R., Rahim, A.A., Howe, S.J., Ward, N.J., Birrell, M.A., Belvisi, M.G., Arbuthnot, P., et al. (2015). In vivo bioimaging with tissue-specific transcription factor activated luciferase reporters. Sci. Rep. *5*, 11842.

Catapult, C.G.T. (2020). Cell and gene therapy Catapult clinical trials database 2019 commentary [online]. https://ct.catapult.org.uk.

Cavero, I., Guillon, J.M., and Holzgrefe, H.H. (2019). Human organotypic bioconstructs from organ-on-chip devices for human-predictive biological insights on drug candidates. Expert Opin. Drug Saf. *18*, 651–677.

Chen, K.T., Pernelle, K., Tsai, Y.H., Wu, Y.H., Hsieh, J.Y., Liao, K.H., Guguen-Guillouzo, C., and Wang, H.W. (2014). Liver X receptor alpha (LXRalpha/NR1H3) regulates differentiation of hepatocyte-like cells via reciprocal regulation of HNF4alpha. J. Hepatol. *61*, 1276–1286.

Chougule, P., and Sumitran-Holgersson, S. (2012). Cytokeratins of the liver and intestine epithelial cells during development and disease. In Cytokeratins - Tools in Oncology, G. Hamilton, ed. (InTech), pp. 118–158.

Collins, S.D., Yuen, G., Tu, T., Budzinska, M.A., Spring, K., Bryant, K., and Shackel, N.A. (2019). In vitro models of the liver: disease modeling, drug discovery and clinical applications. In Hepatocellular Carcinoma, J.E.E. Tirnitz-Parker, ed. (Codon Publications), pp. 47–67.

Dash, A., Simmers, M.B., Deering, T.G., Berry, D.J., Feaver, R.E., Hastings, N.E., Pruett, T.L., Lecluyse, E.L., Blackman, B.R., and Wamhoff, B.R. (2013). Hemodynamic flow improves rat hepatocyte morphology, function, and metabolic activity in vitro. Am. J. Physiol. Cell Physiol. *304*, C1053–C1063.

Delhove, J.M., Buckley, S.M., Perocheau, D.P., Karda, R., Arbuthnot, P., Henderson, N.C., Waddington, S.N., and Mckay, T.R. (2017). Longitudinal in vivo bioimaging of hepatocyte transcription factor activity following cholestatic liver injury in mice. Sci. Rep. *7*, 41874.

Ehrlich, A., Duche, D., Ouedraogo, G., and Nahmias, Y. (2019). Challenges and opportunities in the design of liver-on-chip microdevices. Annu. Rev. Biomed. Eng. *21*, 219–239.

Elmaouhoub, A., Dudas, J., and Ramadori, G. (2007). Kinetics of albumin- and alpha-fetoprotein-production during rat liver development. Histochem. Cell Biol. *128*, 431–443.

Huang, D., Gibeley, S.B., Xu, C., Xiao, Y., Celik, O., Ginsberg, H.N., and Leong, K.W. (2020). Engineering liver microtissues for disease modeling and regenerative medicine. Adv. Funct. Mater. *30*, 1909553.

Komati, R., Spadoni, D., Zheng, S., Sridhar, J., Riley, K.E., and Wang, G. (2017). Ligands of therapeutic utility for the liver X receptors. Molecules *22*, 1–24.

Kriegermeier, A., and Green, R. (2020). Pediatric cholestatic liver disease: Review of bile acid metabolism and discussion of current and emerging therapies. Front. Med. (Lausanne) *7*, 1–15.

Lisowski, L., Dane, A.P., Chu, K., Zhang, Y., Cunningham, S.C., Wilson, E.M., Nygaard, S., Grompe, M., Alexander, I.E., and Kay, M.A. (2014). Selection and evaluation of clinically relevant AAV variants in a xenograft liver model. Nature *506*, 382–386.

Lorvellec, M., Scottoni, F., Crowley, C., Fiadeiro, R., Maghsoudlou, P., Pellegata, A.F., Mazzacuva, F., Gjinovci, A., Lyne, A.M., Zulini, J., et al. (2017). Mouse decellularised liver scaffold improves human embryonic and induced pluripotent stem cells differentiation into hepatocyte-like cells. PLoS One *12*, e0189586.

Ma, L., and Nelson, E.R. (2019). Oxysterols and nuclear receptors. Mol. Cell. Endocrinol. *484*, 42–51.

Mackenzie, C.G., Mackenzie, J.B., and Beck, P. (1961). The effect of pH on growth, protein synthesis, and lipid-rich particles of cultured mammalian cells. J. Biophys. Biochem. Cytol. *9*, 141–156.

Maghsoudlou, P., Georgiades, F., Smith, H., Milan, A., Shangaris, P., Urbani, L., Loukogeorgakis, S.P., Lombardi, B., Mazza, G., Hagen, C., et al. (2016). Optimization of Liver Decellularization Maintains Extracellular Matrix Micro-Architecture and Composition Predisposing to Effective Cell Seeding. PLoS One *11*, e0155324.

Manno, C.S., Pierce, G.F., Arruda, V.R., Glader, B., Ragni, M., Rasko, J.J., Ozelo, M.C., Hoots, K., Blatt, P., Konkle, B., et al. (2006). Successful transduction of liver in hemophilia by AAV-Factor IX and limitations imposed by the host immune response. Nat. Med. *12*, 342–347.

Maqdasy, S., Trousson, A., Tauveron, I., Volle, D.H., Baron, S., and Lobaccaro, J.M. (2016). Once and for all, LXRalpha and LXRbeta are gatekeepers of the endocrine system. Mol. Aspects Med. *49*, 31–46.

Mariotti, V., Strazzabosco, M., Fabris, L., and Calvisi, D.F. (2018). Animal models of biliary injury and altered bile acid metabolism. Biochim. Biophys. Acta Mol. Basis Dis. *1864*, 1254–1261.

Martignoni, M., Groothuis, G.M., and De Kanter, R. (2006). Species differences between mouse, rat, dog, monkey and human CYP-mediated drug metabolism, inhibition and induction. Expert Opin. Drug Metab. Toxicol. *2*, 875–894.

Martinelli, J., Habes, D., Majed, L., Guettier, C., Gonzales, E., Linglart, A., Larue, C., Furlan, V., Pariente, D., Baujard, C., et al. (2018). Long-term outcome of liver transplantation in childhood: a study of 20-year survivors. Am. J. Transpl. *18*, 1680–1689.

Mazza, G., Al-Akkad, W., Telese, A., Longato, L., Urbani, L., Robinson, B., Hall, A., Kong, K., Frenguelli, L., and Marrone, G. (2017). Rapid production of human liver scaffolds for functional tissue engineering by high shear stress oscillation-decellularization. Sci. Rep. *7*, 5534.

Mitro, N., Vargas, L., Romeo, R., Koder, A., and Saez, E. (2007). T0901317 is a potent PXR ligand: implications for the biology ascribed to LXR. FEBS Lett. *581*, 1721–1726.

Nathwani, A.C., Reiss, U.M., Tuddenham, E.G., Rosales, C., Chowdary, P., Mcintosh, J., Della Peruta, M., Lheriteau, E., Patel, N., Raj, D., et al. (2014). Long-term safety and efficacy of factor IX gene therapy in hemophilia B. N. Engl. J. Med. *371*, 1994–2004.

Nayak, N.C., and Mital, I. (1977). The dynamics of alpha-fetoprotein and albumin synthesis in human and rat liver during normal ontogeny. Am. J. Pathol. *86*, 359–374.

Park, R., Leach, W.J., and Arieff, A.I. (1979). Determination of liver intracellular pH in vivo and its homeostasis in acute acidosis and alkalosis. Am. J. Physiol. *236*, F240–F245.

Paulk, N.K., Pekrun, K., Zhu, E., Nygaard, S., Li, B., Xu, J., Chu, K., Leborgne, C., Dane, A.P., Haft, A., et al. (2018). Bioengineered AAV capsids with combined high human liver transduction in vivo and unique humoral seroreactivity. Mol. Ther. *26*, 289–303.

Pollock, A.S. (1984). Intracellular pH of hepatocytes in primary monolayer culture. Am. J. Physiol. *246*, F738–F744.

Pound, P., and Ritskes-Hoitinga, M. (2018). Is it possible to overcome issues of external validity in preclinical animal research? Why most animal models are bound to fail. J. Transl. Med. *16*, 304.

Sellaro, T.L., Ranade, A., Faulk, D.M., Mccabe, G.P., Dorko, K., Badylak, S.F., and Strom, S.C. (2010). Maintenance of human hepatocyte function in vitro by liver-derived extracellular matrix gels. Tissue Eng. Part A *16*, 1075–1082.

Song, Z., Cai, J., Liu, Y., Zhao, D., Yong, J., Duo, S., Song, X., Guo, Y., Zhao, Y., Qin, H., et al. (2009). Efficient generation of hepatocyte-like cells from human induced pluripotent stem cells. Cell Res. *19*, 1233–1242.

Strazzabosco, M., and Boyer, J.L. (1996). Regulation of intracellular pH in the hepatocyte. Mechanisms and physiological implications. J. Hepatol. *24*, 631–644.

Strom, S.C., Davila, J., and Grompe, M. (2010). Chimeric mice with humanized liver: tools for the study of drug metabolism, excretion, and toxicity. Methods Mol. Biol. *640*, 491–509.

Takeishi, K., Collin De L'hortet, A., Wang, Y., Handa, K., Guzman-Lepe, J., Matsubara, K., Morita, K., Jang, S., Haep, N., Florentino, R.M., et al. (2020). Assembly and function of a bioengineered human liver for transplantation generated solely from induced pluripotent stem cells. Cell Rep. *31*, 107711.

Tharp, K.M., and Weaver, V.M. (2018). Modeling tissue polarity in context. J. Mol. Biol. *430*, 3613–3628.

Tresoldi, C., Pellegata, A.F., and Mantero, S. (2015). Cells and stimuli in small-caliber blood vessel tissue engineering. Regen. Med. *10*, 505–527.

Uygun, B.E., Soto-Gutierrez, A., Yagi, H., Izamis, M.L., Guzzardi, M.A., Shulman, C., Milwid, J., Kobayashi, N., Tilles, A., Berthiaume, F., et al. (2010). Organ reengineering through development of a transplantable recellularized liver graft using decellularized liver matrix. Nat. Med. *16*, 814–820.

Van Haasteren, J., Hyde, S.C., and Gill, D.R. (2018). Lessons learned from lung and liver in-vivo gene therapy: implications for the future. Expert Opin. Biol. Ther. *18*, 959–972.

Vernetti, L.A., Senutovitch, N., Boltz, R., Debiasio, R., Shun, T.Y., Gough, A., and Taylor, D.L. (2016). A human liver microphysiology platform for investigating physiology, drug safety, and disease models. Exp. Biol. Med. (Maywood) *241*, 101–114.

Xu, J., Hu, Y., Wang, J., Zhou, J., Zhang, T., and Yu, H. (2007). Immunohistochemical characterization of hepatic stem cell-related cells in developing human liver. Front. Med. China *1*, 264–268.

You, Z., Zhou, L., Li, W., Huang, C., and Du, Y. (2019). Mechanical microenvironment as a key cellular regulator in the liver. Acta Mech. Sin. *35*, 289–298.

Yusa, K., Rashid, S.T., Strick-Marchand, H., Varela, I., Liu, P.Q., Paschon, D.E., Miranda, E., Ordonez, A., Hannan, N.R., Rouhani, F.J., et al. (2011). Targeted gene correction of alpha1-antitrypsin deficiency in induced pluripotent stem cells. Nature *478*, 391–394.

Zabaleta, N., Hommel, M., Salas, D., and Gonzalez-Aseguinolaza, G. (2019). Genetic-based approaches to inherited metabolic liver diseases. Hum. Gene Ther. *30*, 1190–1203.

iScience, Volume *23*

Supplemental Information

An *In Vitro* Whole-Organ Liver Engineering for Testing of Genetic Therapies

Maëlle Lorvellec, Alessandro Filippo Pellegata, Alice Maestri, Chiara Turchetta, Elena Alvarez Mediavilla, Soichi Shibuya, Brendan Jones, Federico Scottoni, Dany P. Perocheau, Andrei Claudiu Cozmescu, Juliette M. Delhove, Daniel Kysh, Asllan Gjinovci, John R. Counsell, Wendy E. Heywood, Kevin Mills, Tristan R. McKay, Paolo De Coppi, and Paul Gissen

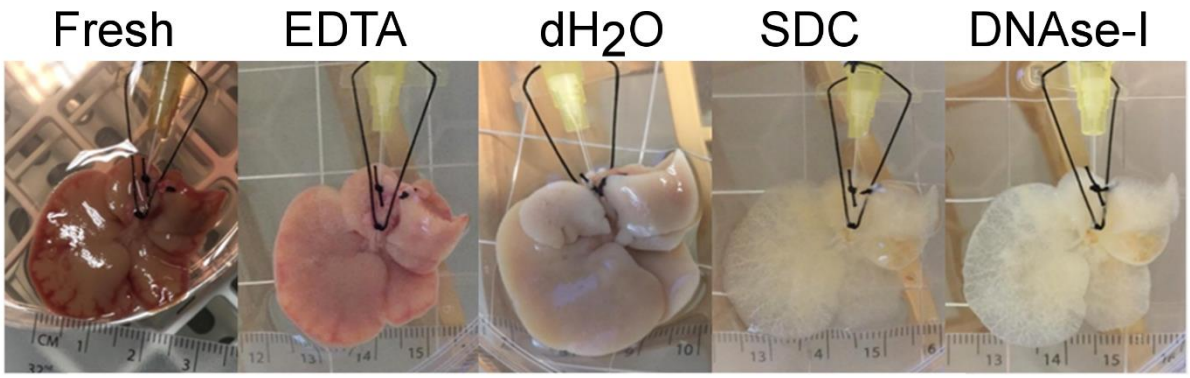

Figure S1: Mouse liver decellularisation by DET method. Related to Figure 1. Macroscopic appearance of a mouse liver scaffold during the decellularisation process. First, the liver is perfused with EDTA to reduce clotting. Then it is perfused with demineralized water (dH_2O) and becomes blanched. After perfusion with sodium deoxycholate (SDC) followed by DNAseI treatment, the liver becomes transparent. Finally, it is washed with dH_2O. Scale bar 5 mm.

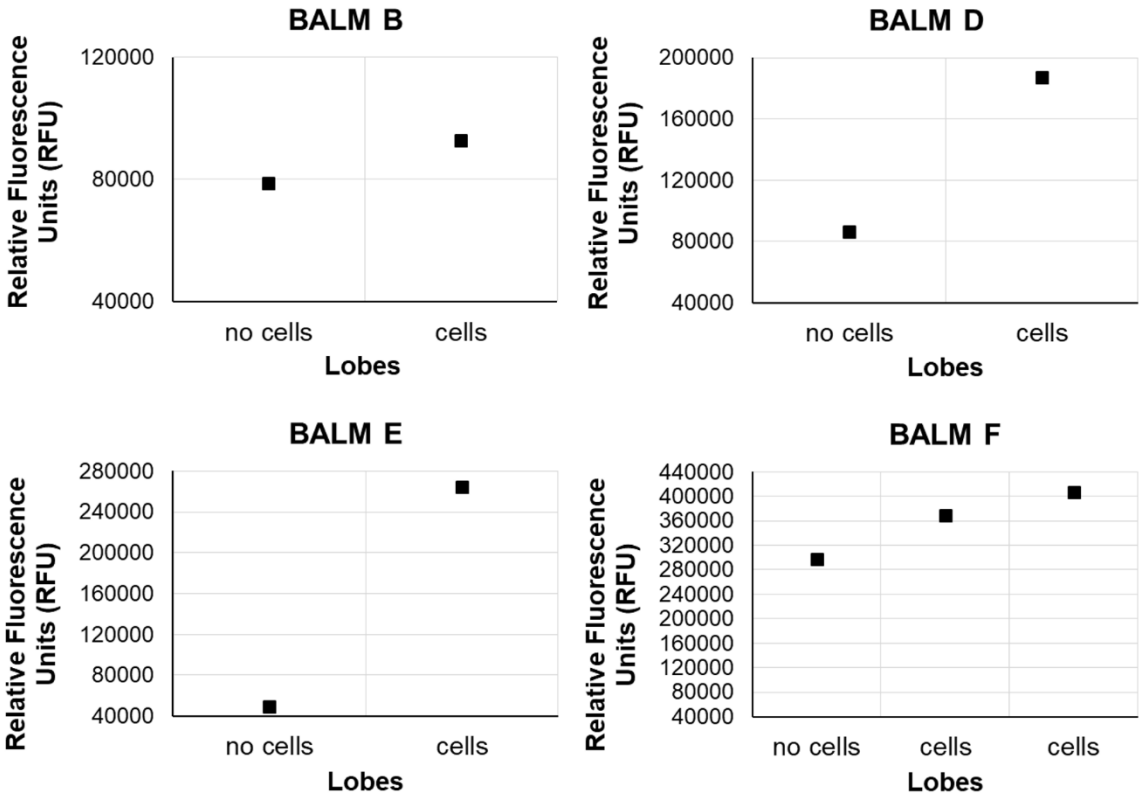

Figure S2: Cell viability on day of harvest in BALMs. Related to Figure 2. Cell viability in individual lobes seeded (cells) or unseeded (no cells) with DECs for individual BALMs evaluated by PrestoBlue assay on the day of harvest: d26 for BALM B, D, d27 for BALM E and d20 for BALM F. Fluorescence values from seeded lobes demonstrate that cells are still alive within the scaffold at the time of harvest.

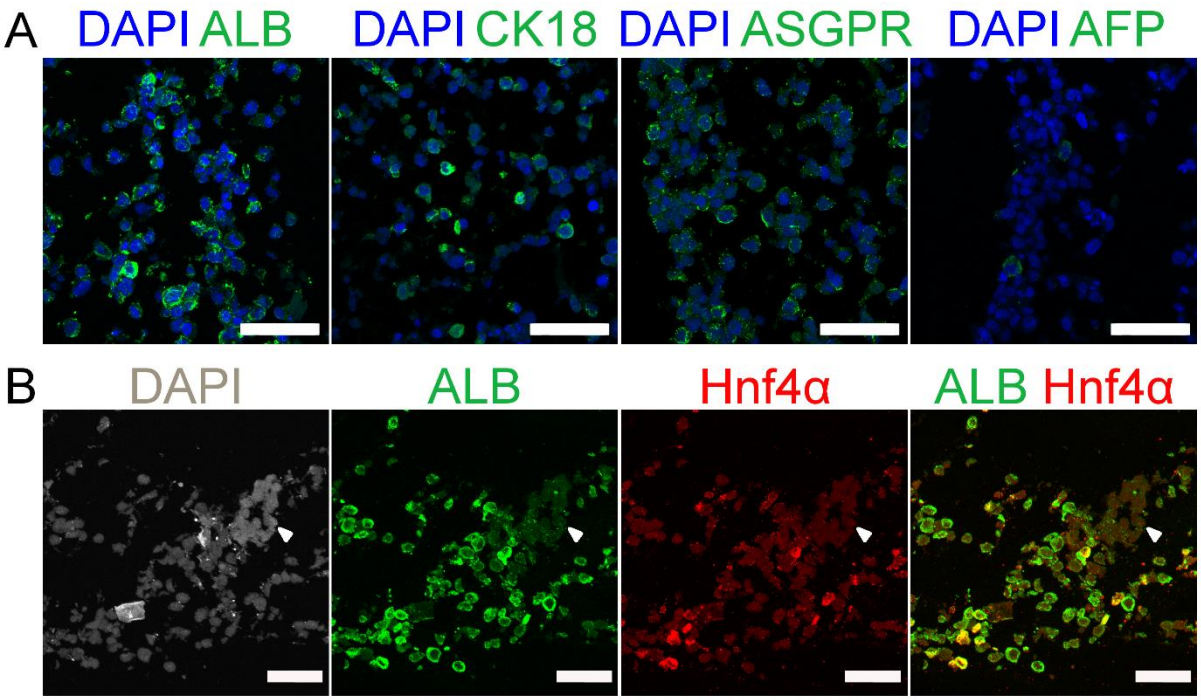

Figure S3: hiHEPs and HUVECs in BALM. Related to Figure 3. (A) Hepatocyte markers expression by hiHEPs in BALM on day 26 of differentiation. Higher magnfication images of merged channels maximum intensity projection of z-stacks correspond to the higher magnification images of Figure 3.A. Hepatocyte sinusoidal membrane protein ASGPR is localised at the cell membrane. Nuclei stained with DAPI. Scale bar 50 µm. (B)**.** Immunostaining of the hepatocyte markers ALB and Hepatocyte nuclear Factor 4α (HNF4α) show expression in the hiHEPs located in the parenchyma, but none in the HUVECs located in the blood vessel (arrowhead). The images are maximum intensity projections of z-stacks. Nuclei stained with DAPI. Scale bar 50µm.

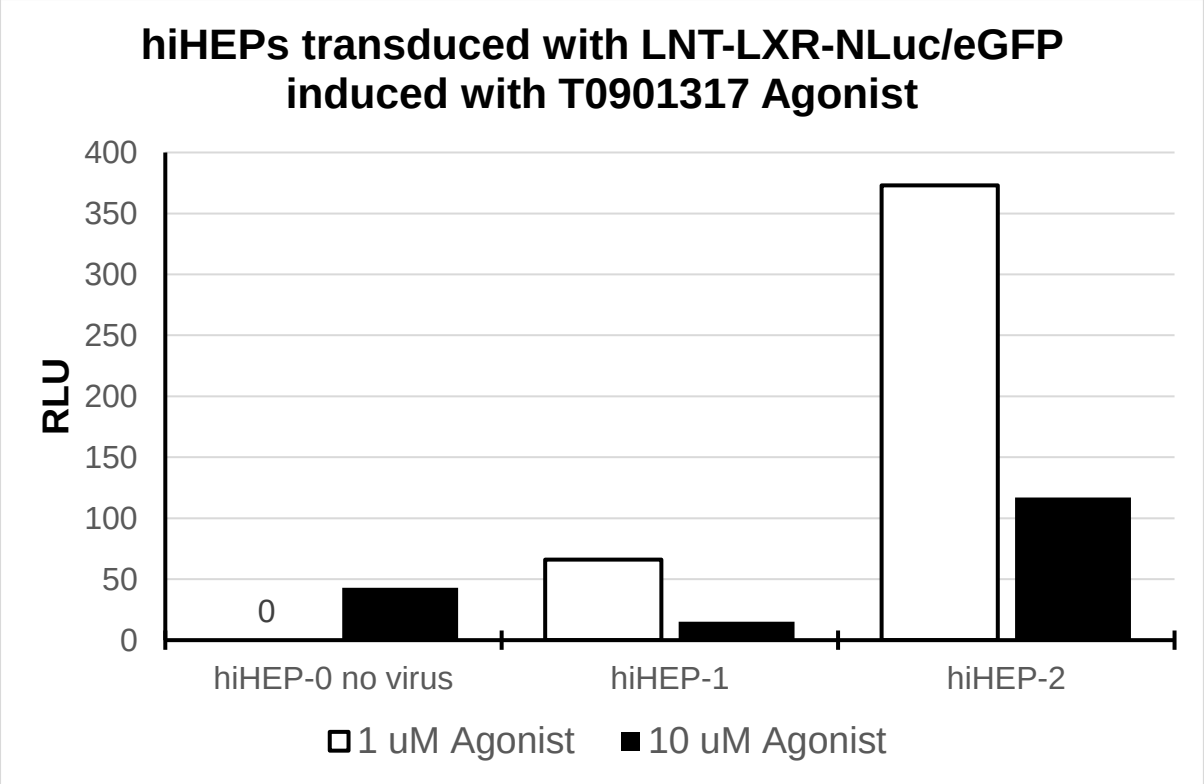

Figure S4. **hiHEPs transduced with LNT-LXR-Nluc/eGFP in 2D culture. Related to Figure 4**. hiHEPs cultured in 2D were transduced with LNT-LXR-Nluc/eGFP for 24h followed by 24h incubation with 1 or 10 µM T0901317 agonist (1 well with no virus, hiHEP-0, and 2 wells with, hiHEP-1 and 2, for each agonist condition). Bioluminescence (RLU) of secreted nanoluciferase in the media shows higher luciferase secretion in hiHEPs induced with 1 than 10 µM agonist.

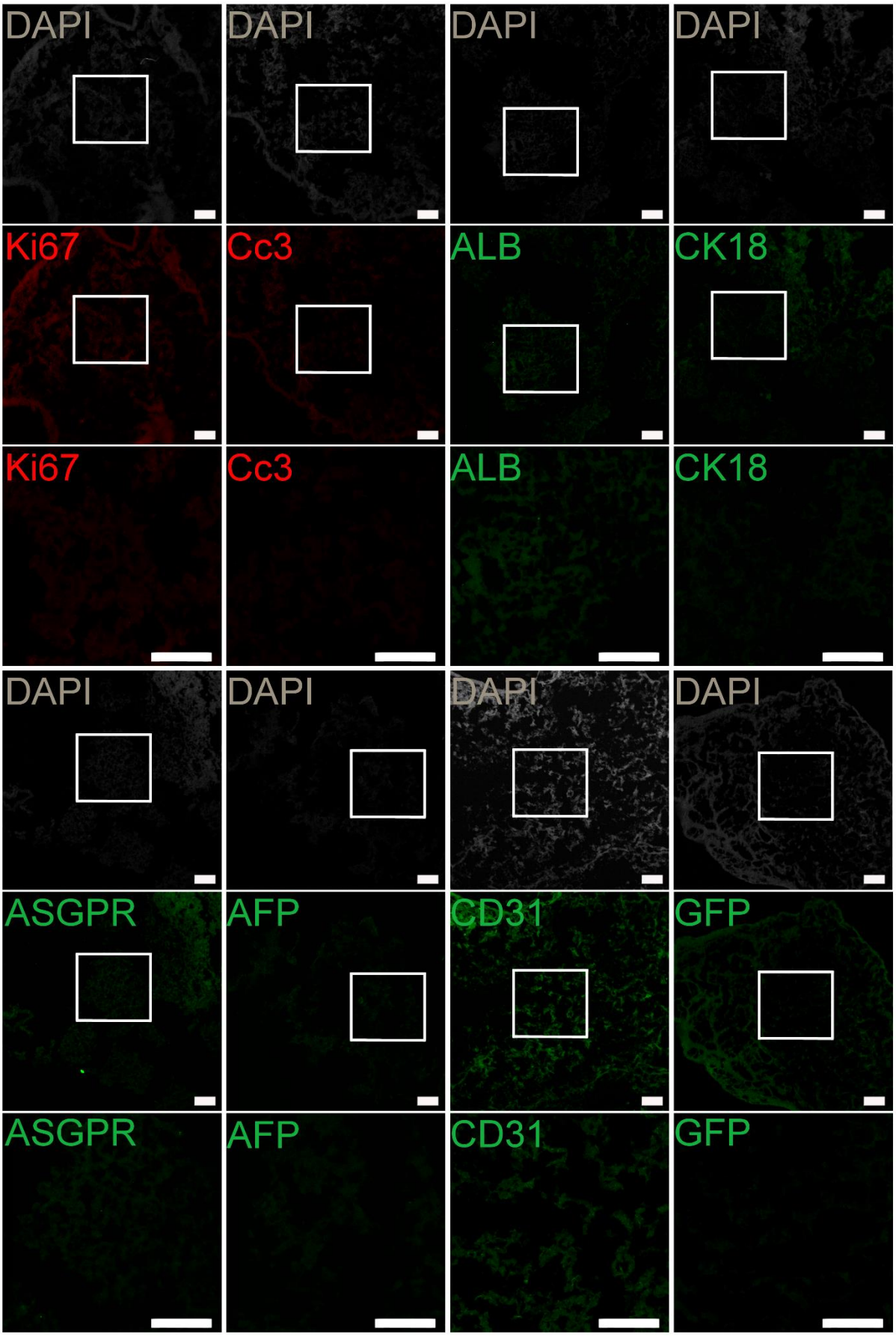
DAPI
DAPI
DAPI
DAPI
Ki67
Cc3
ALB
CK18
Ki67
Cc3
ALB
CK18
DAPI
DAPI
DAPI
DAPI
ASGPR
AFP
CD31
GFP
ASGPR
AFP
CD31
GFP

Figure S5. Immunodetection of different markers on decellularised lobes with no cells. **Related to Figures 2, 3 and 4**. Non seeded lobes were stained and imaged with the same settings as the seeded lobes for each marker. Some background staining is visible and differences between each marker is due to the different primary antibodies as well as different gain used; however, the diffuse background signal observed is much lower than the primary antibodies signal observed for the seeded lobes. Higher magnification images in the middle and bottom panels correspond to the delineated lower magnification images. Nuclei stained with DAPI. Scale bar 50 μm.

DAY OF DIFFERENTIATION	BALM	ALB AREA	AFP AREA	ALB AREA / HOUR	AFP AREA / HOUR	ALB/AFP
19	A	87125	46293	565000	300000	1.882034
	B	86157	32307	642000	241000	2.666821
	C	U	U	U	U	U
21-22	A	U	U	U	U	U
	B	469906	44502	1240000	117000	10.55921
	C	402133	67374	1510000	253000	5.968667
25	A	592836	6344	1540000	16500	93.4483
	B	U	U	U	U	U
	C	U	U	U	U	U

Table S1: Area values and Area/hour for Albumin (ALB) and Alpha-fetoprotein (AFP), and ALB/AFP ratios per day of differentiation for each BALM. Related to Figure 3. Due to the unknown number of cells surviving in the scaffold the ALB Area/AFP Area ratios were calculated for comparison between time points and BALMs. U = media unavailable.

SAMPLE	NANOLUC LUCIFERASE ASSAY			BIOLUMINESCENCE IMAGING DAY 25 PH/SEC		
	MEDIA RLU/ML/H DAY 19	MEDIA RLU/ML/H DAY 25	FOLD CHANGE	BACKGROUND READING	5 MIN AFTER SUBSTRATE PERFUSION	TOTAL FLUX
BALM 0 no virus	15.3	28.9	1.89			
BALM 1	0.0185	4650	251000	9.6e4	4.14e7	4.13e7
BALM 2	25.1	482	19.2	1.78e5	9.11e7	9.09e7
BALM 3	0.0192	87.1	4540	2.86e5	3.20e8	3.20e8
PHHs no virus	Media 48h after agonist activation	6.25	1.0			
PHHs + pLNT-LXR-Nluc/eGFP		83700	13400			

Table S2: Bioluminescence values before and after transduction and agonist activation for each BALM and PHHs. Related to Figure 4. NanoLuc luciferase assay values in Relative Light Unit/ml/hour (RLU/ml/h)(left); Live imaging of BALMs values in photons/sec (ph/sec) (right).

PRIMARY ANTIBODIES					
ANTIGEN	TYPE	COMPANY	FIXATION	BLOCKING SOLUTION	DILUTION
AFP	Mouse monoclonal	A8452. Sigma-Aldrich	Methanol (MetOH)[a] or ParaFormaldehyde (PFA) +MetOH	2x casein (Vector Laboratories) in PBS or 1% donkey serum (Serotec Ltd) + 1% triton X-100 (Sigma) in PBS	1:200
ALB	Mouse monoclonal	A6684. Sigma-Aldrich	MetOH [a] or PFA+MetOH	2x casein (Vector Laboratories) in PBS or 1% donkey serum (Serotec Ltd) + 1% triton X-100 (Sigma) in PBS	1:200
ASGPR	Mouse monoclonal	MA1-40244. Thermofisher scientific	PFA+MetOH	1% donkey serum (Serotec Ltd) + 1% triton X-100 (Sigma) in PBS	1:100
CC3	Rabbit polyclonal	9661. Cell Signaling Technology	PFA	1% goat serum (Sigma) + 1% triton X-100 (Sigma) in PBS	1:100
CD31	Mouse monoclonal	MA5-13188. Thermofisher scientific	PFA	10% donkey serum (Serotec Ltd) + 0.5% triton X-100 (Sigma) in PBS	1:100
CK-7	Mouse monoclonal	18-0234. Thermofisher scientific	PFA+MetOH	1% BSA (Serotec Ltd) + 0.5% triton X-100 (Sigma) in PBS	1:100
CK-18	Mouse monoclonal	M7010. Dako	PFA+MetOH	1% donkey serum (Serotec Ltd) + 1% triton X-100 (Sigma) in PBS	1:100
CK-19	Rabbit polyclonal	Ab15463. Abcam	PFA+MetOH	1% donkey serum (Serotec Ltd) + 1% triton X-100 (Sigma) in PBS	1:100
GFP	Rabbit polyclonal	Ab290. Abcam	PFA	1-3% BSA (Sigma) + 0.5% triton X-100 (Sigma) in PBS	1:200
HNF4α	Rabbit polyclonal	Sc8987. Santa-Cruz biotechnology	MetOH [a] or PFA+MetOH	2x casein (Vector Laboratories) in PBS or 1% donkey serum (Serotec Ltd) + 1% triton X-100 (Sigma) in PBS	1:200
Ki-67	Rabbit polyclonal	Ab15580. Abcam	PFA	1% goat serum (Sigma) + 1% triton X-100 (Sigma) in PBS	1:100
SOX-17	Goat polyclonal	AF1924. R&D Systems	PFA or PFA+MetOH	1% donkey serum (Serotec Ltd) + 1% triton X-100 (Sigma) in PBS	1:100

SECONDARY ANTIBODIES		
TYPE	COMPANY	DILUTION
Alexa Fluor 488 GOAT anti MOUSE	A-11029. ThermoFisher scientific	1:500
Alexa Fluor 568 GOAT anti RABBIT	A-11036. ThermoFisher scientific	1:500
Alexa Fluor 568 DONKEY anti RABBIT	A-10042. ThermoFisher scientific	1:500
Alexa Fluor 488 DONKEY anti MOUSE	A-21202. ThermoFisher scientific	1:500
Alexa Fluor 488 DONKEY anti GOAT	A-11055. ThermoFisher scientific	1:500

Table S3: List of antibodies, their dilution factor and blocking buffer used. Related to Figures 2, 3, and 4.
[a] preferred fixation.

PROTEIN	PEPTIDE SEQUENCE	RETENTION TIME (MIN)	PRECURSOR ION (M/Z)	PRODUCT ION (M/Z)	CONE VOLTAGE (V)	COLLISION ENERGY	SOURCE
AFP	TFQAITVTK	3.75	504.7899	632.3978	35	18	Genscript, USA
ALB	FQNALLVR	4.19	480.7849	685.3824	35	17	Genscript, USA

Table S4. Multiple Reaction Monitoring parameters (MRM). Related to Figure 3.
M = mass Z= charge number of ions V = volt.

TRANSPARENTS METHODS

Harvest of organs.

This study was carried out following the recommendations in the Animal (Scientific Procedures) Act 1986. The Home Office approved the study protocol (licence number 70/2716). Organs were obtained from CD-1 mice, any sex, aged 3 to 4 months. Livers were harvested as previously described (Maghsoudlou et al., 2016, Lorvellec et al., 2017). Briefly, immediately following sacrifice by cervical dislocation, the abdominal cavity was opened. The inferior vena cava (IVC) was ligated using a 3/0 silk suture above the right renal vein, whereas the superior vena cava was cut open to allow fluid to flow out during following decellularization. A 24G cannula (Introcan®-W Certo 24G, Braun, Germany) was inserted to the portal vein (PV) and secured with a 3/0 silk suture (FST, UK), fixing its tip just after the formation of the PV from superior mesenteric and splenic veins. The liver was carefully dissected from surrounding tissues, avoiding injury to the liver capsule, and was transferred to a petri dish filled with 2% EDTA solution. The liver was assessed for injury by injection of EDTA through the cannula, showing sufficient perfusion of each lobe, while also preventing clotting of blood in the microvasculature.

Cells and culture conditions.

The hiPSCs line is a generous gift from Prof. L. Vallier (male donor, corrected A1ATD-hiPSCs (Yusa et al., 2011)). This line has successfully been used to generate hepatocyte-like cells in 2D and 3D cultures (Song et al., 2009, Yusa et al., 2011, Lorvellec et al., 2017). Stem cells were cultured in mTeSR Plus medium (Stem cell technologies, UK) on matrigel growth factor reduced (Corning, UK) coated dishes. Media was changed daily or every 2 days and cells were split mechanically every 3-5 days. All cells were tested monthly for the lack of mycoplasma contamination using the MycoAlert Mycoplasma Detection Kit (Lonza, UK).

Primary Human Hepatocytes (PHHs, 66 years old male donor) were purchased from Biopredic International (France) as confluent monolayers (*ca.* 3.08×10^5 cells per well) in 24-well plates pre-coated with a single film of collagen. PHHs were maintained in Maintenance media and were transferred to Induction media (Williams E with Glutamax-I added with 100 IU/ml of penicillin, 100 µg/ml of streptomycin, 4 µg/ml of bovine insulin and $5x10^{-5}$ M of hydrocortisone hemisuccinate) for the experiment (Biopredic, France).

Human umbilical vein endothelial cells (pooled donors) were purchased from Lonza (UK) and culture in Endothelial Cell Growth Medium 2 (ECGM2, C-22011, Promocell, UK). Cells were expanded for stock generation and frozen at passage 3.

HEK293T viral producer cells (Counsell et al., 2018) were cultured in DMEM high glucose with Glutamax, 10% FBS and 1% penicillin/streptomycin (ThermoFisher Scientific, UK).

All cells were cultured in a 5% CO_2:95% air humidified atmosphere at 37°C.

Bioreactor.

The bioreactor chamber was composed of a polytetrafluoroethylene body and a polycarbonate lid provided with silicone gaskets and polypropylene connectors. The perfusion system was composed of Pharmed tubings (Cole Parmer, UK), a peristaltic pump (Ismatec Reglo Digital 4-channel 6-rollers; Cole Parmer, UK), and bubble trap (Omnifit Ltd., UK). The air system was composed of a 5% CO2 Air tank connected to flowmeter (Cole Parmer, UK) and Pyrex bottles (Cole Parmer, UK) with caps that allowed sterile tubing connections (Omnifit Ltd., UK). Temperature was controlled using hot plate (Cole Parmer, UK) underneath the bioreactor chamber and the pyrex bottles. pH and temperature monitoring were performed using an invasive sensing system with a sterile dip sensor (Easyferm plus Arc Air 120, Hamilton, UK) directly in contact with the media in the chamber. This sensor is an arc intelligent probe with an integrated transmitter and a Bluetooth connection. It connects to a computer using a wireless adapter (ARC WI 1G Adapter BT; Hamilton, UK) and a wireless converter (Arc Wireless Converter BT; Hamilton, UK).

Decellularisation protocol.

Mouse livers were decellularised as previously described using the Detergent Enzymatic Treatment (DET) method with a few modifications (Maghsoudlou et al., 2016, Lorvellec et al., 2017). Briefly, the PV was connected to a peristaltic pump (Masterflex, UK) perfused with 2% EDTA for 15 min and then with demineralised water (dH_2O) (18.2 mΩ/cm) for 24 hours at room temperature followed by 4% sodium deoxycholate (SDC) (Sigma-Aldrich, UK) for 4h. The liver was rinsed overnight with dH_2O. The next day, the liver was perfused with 2,000 kU solution of deoxyribonuclease-I (DNase-I, Sigma-Aldrich, UK) in 1 M sodium chloride for 4h. Finally, the liver was perfused with dH_2O for 48h. All the reagents were perfused at a rate of 3 ml/min at room temperature. The obtained mouse liver scaffolds were sterilised by gamma-irradiation before seeding cells.

Differentiation of hiHEPs in BALM.

hiPSCs were differentiated into hepatocyte-like cells as described with a few modifications (Sullivan et al., 2010, Lorvellec et al., 2017). Stem cells were cultured until 80-90% confluency. They were split 1/6 on matrigel

coated dishes and let rest for 1 day with daily change of mTeSR Plus. They were then incubated with priming media Roswell Park Memorial Institute (RPMI) (Thermofisher, UK) and 1x B27 (ThermoFisher, UK) with 100 ng/ml activin A (Peprotech, UK) and 50 ng/ml Wnt3a (R&D systems, UK) for 3 days followed by 2 days incubation in 100 ng/ml activin A alone. At this point, day 6 of differentiation, Definitive Endoderm-like Cells (DECs) were harvested with enzyme-free Cell Dissociation Buffer (ThermoFisher, UK), avoiding remaining stem cells colonies and seeded in specification medium SR/DMSO (KO/DMEM containing 20% KO Serum Replacement, 1 mM L-glutamine, 1% non-essential amino acids, 0.1 mM β-mercaptoethanol (ThermoFisher Scientific, UK), and 1% dimethyl sulfoxide (Sigma-Aldrich, UK)) with 10 µM rock inhibitor Y-27632 (Sigma-Aldrich, UK) overnight. DECs, differentiated in parallel, were fixed and analysed afterwards by immunofluorescence staining for Sox17, an endoderm marker, as a low percentage of Sox17 cells at endoderm stage predicts poor hepatocyte differentiation. Differentiation batches that were less than 15% Sox17 positive were excluded from this study. The decellularised mouse liver scaffolds generated by DET were visually evaluated for their ability to be perfused through their vasculature by injecting a coloured media via the catheter in their portal vein. Only the lobes able to be perfused were seeded with DECs. DECs at 2.5-5x10^6 / 200 µl were injected into 3 points of one up to three decellularised lobes with a 29G microfine syringe (BD, UK), this was repeated 3 times drawing up the cells leaking out of the lobe after each injection. A minimum of 5x10^6 cells up to 20x10^6 cells was seeded per scaffold. The seeded decellularised liver was placed into the chamber of the bioreactor with 20 ml of specification media with rock inhibitor and connected to the circuit via its catheter (primed with 10 ml of specification media with rock inhibitor). The flowmeter controlling the gas flow was set at 50 ml/min and the hotplate at 48℃ so that the temperature of the media inside of the chamber was 37℃. The next day, the peristaltic pump was started at a flow rate of 1 ml/min, the media of the chamber was changed to fresh media without rock inhibitor and then every 2 days till day 11 of differentiation. During hepatic maturation 1, growth factors were added every 2 days: 10 ng/ml hepatocyte growth factor HGF and 20 ng/ml oncostatin M (Peprotech, UK), and media was changed every 4 days up to day 17 of differentiation with L-15 medium supplemented with 8.3% FBS, 8.3% tryptose phosphate broth, 10 µM hydrocortisone 21-hemisuccinate, 1 µM insulin (Sigma-Aldrich, UK), 2 mM glutamine, 10 ng/ml HGF and 20 ng/ml oncostatin M. During the hepatic maturation 2, growth factors were added every 2 days: 10 ng/ml HGF and 20 ng/ml oncostatin M, and media was changed every 2 or 4 days up to day 27 of differentiation with William's E medium (Invitrogen, UK) supplemented with 10mM nicotinamide, 17 mM NaHCO3, 0.2 mM AAP2, 20 mM Hepes (Sigma-Aldrich, UK), (Sigma), 6.3 mM NaPyruvate (Invitrogen), 14 mM Glucose (ThermoFisher Scientific, UK), 1x ITS +Premix (Corning, UK), 0.1 µM Dexamethasone (R&D Systems, UK), , 2 mM glutamine, 10 ng/ml HGF and 20 ng/ml oncostatin M. All media after the endoderm stage were supplemented with 100 µg/ml of the antimicrobial Primocin (Invivogen, France).

Coculture of hiHEPs and HUVECs in BALM.

Only the scaffolds able to be perfused were seeded with HUVECs (passages 5-6 maximum), 4 days before seeding with DECs (at day 2 of differentiation). 5x10^6 HUVECs were resuspended into 1 ml of ECGM2 with 10 µM rock inhibitor Y-27632 and slowly perfused with a 1 ml syringe through the PV catheter. The seeded decellularised liver was placed into the chamber of the bioreactor with 20 ml of ECGM2 with rock inhibitor and connected to the circuit via its catheter (primed with 10 ml of ECGM2 with rock inhibitor) overnight. The flowmeter controlling the gas flow was set at 50 ml/min and the hotplate at 48℃ so that the temperature of the media inside of the chamber is 37℃. The next day, the peristaltic pump was started at a flow rate of 0.5 ml/min for half a day and then switched to 1 ml/min. The media of the chamber was changed to fresh media without rock inhibitor and then every 2 days till day 6 of differentiation, when the scaffold was disconnected from the bioreactor and seeded with DECs as described in the previous paragraph. When the scaffold co-seeded with HUVECs and DECs was placed back in the bioreactor, the peristaltic pump was started at a flow rate of 0.5 ml/min for half a day and then switched to 1ml/min. All media were then composed of half media needed for DECs and half ECGM2 till harvesting at day 20-21 of differentiation.

Presto blue cell viability assay.

PrestoBlue™ Cell Viability Reagent (Invitrogen, UK) is a resazurin-based membrane permeable solution, which, upon reduction, forms a red fluorescent compound called resorufin via mitochondrial enzymes of viable cells in the tested systems. As a consequence, the reagent exhibits a change in colour, as well as a shift in its fluorescence. To perform the test the liver scaffolds were disconnected from the chamber of the bioreactor, and dissected into individual lobes in sterile conditions. Subsequently each lobe was cut and incubated in 500 µl of media with 50 µLof Presto Blue reagent in a 24 well dish for 4 h at 37ºC, 5% CO_2. 100 µl of media for each lobe was collected and the fluorescence was measured in a 96w plate at λ_{ex} 544 nm and λ_{em} 620 nm using an Envision Multimode Reader and Wallac EnVision software (Perkin Elmer, UK).

Samples preparation for immunostaining.
The liver scaffolds were disconnected from the chamber of the bioreactor, dissected into individual lobes and embedded in OCT compound (VWR, UK) on a bath of isopentane (Sigma-Aldrich, UK) cooled in liquid nitrogen and sectioned at 4-6 µm on a cryostat (Leica CM1950). A minimum of 30 and up to 60 cryosections were sectioned per lobe and were stored at -80℃.

Haematoxylin & Eosin staining.
Haematoxylin & Eosin (H&E) staining was performed as previously described (Sullivan et al., 2010, Lorvellec et al., 2017). Cryosections were fixed in 4% PFA in PBS for 15 min, rinsed with PBS followed by tap water. Sections were incubated with Hematoxylin QS (Vector Laboratories, UK) for 1-2 min, rinsed with tap water for 5 min, and incubated with Eosin Y solution (Sigma-Aldrich, UK) for 30 sec. They were dehydrated with 95% then 100% EtOH, dipped in HistoClear (ThermoFisher Scientific, UK) and mounted in a non-aqueous mounting medium.

Immunofluorescence staining.
Immunofluorescence staining was performed as previously described (Sullivan et al., 2010, Lorvellec et al., 2017). Briefly, cryosections were fixed in 4% paraformaldehyde (PFA) for 15 min alone, methanol for 8-10 min alone or 4% PFA followed by methanol depending on the primary antibody. They were quenched with 10 mM NH_4Cl for 10 min, permeabilised in 0.5% Triton X100 for 15 min, and blocked in appropriate blocking buffer for 1h. After overnight incubation with the primary antibody, samples were incubated with the appropriate AlexaFluor-conjugated secondary antibodies. See Table S3 for antibodies dilutions and blocking solutions (Lorvellec et al., 2017), counterstained and mounted using Vectashield Vibrance with DAPI (Vector Laboratories, UK).

Microscopy.
At least 3 BALMs per type of experiment were analysed. All the seeded lobes as well as a minimum of two non-seeded lobes per BALM were examined and at least 3 random cryosections per lobe per staining were imaged. Most representative images were selected. All immunofluorescence images were acquired using Leica TCS SPE3 and SP5 confocal microscopes using 20x and 40x objectives. Leica Application Suite Advanced Fluorescence software was used for basic analysis of the confocal images. The images of H&E staining were captured with a Zeiss Axioplan2 microscope using 20x and 40x objectives. Scales for H&E and confocal images of merged channels of maximum intensity projection of z-stacks were generated using ImageJ v1.50d (Schneider et al., 2012).

Detection of ALB/AFP proteins in BALM media.
1 ml of BALM media samples were spiked with intact yeast enolase protein at 0.6 mg/ml as an internal standard (Sigma-Aldrich, UK) and filtered using 10 kDa molecular weight cut-off filter (Millipore, UK). Concentrated solutes were diluted to 1 ml with ddH_2O, precipitated with 5 volumes of ice-cold acetone (2 h, -20ºC), and centrifuged for 10 min at 18,928g. The resulting pellet was resolubilised in 50 ml of 70% formic acid, and incubated at 4ºC for 2h. 500 µL of ddH_2O was added before freeze-drying overnight at -40ºC.
Samples were denatured with 160 µL of denaturating buffer (100 mM Tris, 6 M urea, 2 M thiourea, 2% w/v ABS-14 pH 7.8), disulphide bridges reduced by adding 12 µl 0.2 M 1,4-dithioerythriol (1 h, RT) and alkylated using 24 µl 0.2 M iodacetamide (45 min, RT). The reaction was quenched with 1320 µl of ddH_2O before tryptic digestion (0.1 mg/ml trypsin, 16 h, 37ºC). After digestion, samples were desalted using 100 mg /1ml isolute C18 cartridges (Biotage, Sweden). Peptides were dried in a rotational evaporator for 9 h at room temperature. Samples were then reconstituted in 100 µL of 3% acetonitrile with 0.1% formic acid. 10 µL was injected for LC-MS/MS analysis using a ACQUITY UPLC coupled to a Xevo TQ-S triple quadrupole mass spectrometer (Waters, UK). Chromatographic separation was achieved over a 10 min gradient using a Waters ACQUITY UPLC TM BEH C18 column (1.7UM, 21x50mm) maintained at 40℃ (Heywood et al., 2015). Quality controls of human plasma spiked in culture media were run in triplicate at the start and end of every run.
Tryptic peptides with sequences unique to human albumin (ALB): FQNALLVR and human alpha-fetoprotein (AFP): TFQAITVTK (Mazzacuva et al., 2019), were measured using multiple reaction monitoring (MRM) (Table S4). Custom-synthesised peptides (Genscript, USA) were used to optimise peptide detection and determine the retention time and identify with maximum accuracy the correct peptides. Data was acquired using Waters MassLynx V4.2 software.
The area of the peak values was obtained for 100 µl analysed per 1 ml of sample by LC-MS/MS. Areas/hour values were calculated by multiplying the area by the amount of media harvested and divided by the time the media was kept in BALM. The number of cells being unknown, the ALB area/ AFP area ratios were calculated for comparison between time points and BALMs. 3 different BALMs were analysed from d19 to d25.

Lentiviral reporter production and titering.
The pLNT-LXR-Nluc/eGFP lentiviral construct consists of a synthetic promoter made up of eight serial LXR minimal binding elements driving the expression of the adenoviral E1A-derived polII-binding minimal promoter. Briefly, the LXR binding sequences were *de novo* synthesised (Aldevron, USA) then cloned into the Gateway shuttle vector (B*am*HI/E*co*RI) pENTR-MP containing the E1A minimal promoter cloned into the vector X*ho*I site. Following Sanger sequencing confirmation, the LXR promoter was cloned into the parental lentiviral vector pLNT-GW-NLuc-F2A-eGFP using the Gateway LR clonase II (Invitrogen, UK) reaction to generate the pLNT-LXR-Nuc/eGFP vector. Clones were selected by endonuclease restriction and subsequent Sanger sequencing from a cPPT specific primer specific primer (5' GTGCAGGGGAAAGAATAGTAG3'). Upon activation, this LXR promoter drives both the expression of the NanoLuc luciferase for live bioluminescence imaging and luciferase assay of the culture media, and eGFP expression for live fluorescence imaging and immunofluorescence staining.
Lentivirus production and titering were performed as previously described (Vink et al., 2017). Briefly, HEK293T viral producer cells were seeded overnight at 1.8×10^7 cells per T175 cm^2 flask and transfected using 40 µg pLNT-LXR-Nluc/eGFP, 10 µg pMD2.G. (VSV-G envelope plasmid, Addgen plasmid # 12559), and 30 µg pCMVΔ R8.74 (gag-pol packaging plasmid, Addgen plasmid # 22036) pre-complexed with 1 µl polyethylenimine (10 mM) (Sigma-Aldrich) in OptiMEM for 4 h. Transfection media was replaced with DMEM high glucose with Glutamax, 10% FBS and 1% penicillin/streptomycin, and viral supernatant collected at 48 and 72 hours, filter-sterilized (0.22 µM) through a PES membrane, and ultracentrifuged for 2 hours at 66802g at 4°C. Pellets were resuspended in 200 µl of OptiMEM and stored at − 80 °C.
Viruses were titered using $5x10^4$ HEK293T per well of a 24-well plate and cells were transduced with serial dilutions of concentrated virus. Cells were split once and 100 ng of DNA extracted 6-7 days after transfection was used and the presence of viral copies detected by qPCR using LTR probe and primers (LTR-F: 5'-TGTGTGCCCGTCTGTTGTGT-3', LTR-R: 5'-GAGTCCTGCGTCGAGAGAGC-3', LTR-Probe: 5'-(FAM)-CAGTGGCGCCCGAACAGGGA-(3BHQ_1)-3') compared to control plasmid concentrations (10^3 to 10^7). Vectorial copy number (VCN) was calculated by dividing the mean quantity value of lentiviral genomes by 15200 (Human genome copies per 100 ng DNA). To obtain the viral titres, the VCN was then multiplied by the number of cells and the volume of virus added (ml). Subsequently, the results from different dilutions were averaged to obtain the final titre value (Charrier et al., 2011).

AAV reporter.
The rAAV-LK03-CMV-eGFP vectors were kindly provided by Leszek Lisowski (Lisowski et al., 2014). Recombinant AAV vectors were produced using HEK293 cells and by packaging AAV2-based genomes in a rAAV-LK03 serotype. Production was made via a three-plasmid transfection as described elsewhere (Grimm et al., 2008). The vectors used in the study were titered by quantitative PCR targeting the WPRE sequence as described previously (Cunningham et al., 2008).

PHHs transduction by Lentivirus.
$3.08x10^5$ PHHs per well of 24-well plate were transduced with $3.08x10^5$ viral particles for 24h in induction media with 5ug/ml of polybrene (Sigma-Aldrich, UK). After transduction, wells were rinsed twice with PBS and fresh induction media with 1 µM T0901317 agonist was added for 48h. The media collected at 48h was assayed for NanoLuc luciferase activity.

BALM viral transduction.
BALMs (only seeded with DECs) were transduced at day 21 of differentiation with rAAV-LK03-CMV-eGFP and BALMs at day 19 of differentiation with LNT-LXR-Nluc/eGFP. $1.6x10^4$ to $3.2x10^4$ viral particles of rAAV-LK03-CMV-eGFP per the number of DECs seeded or 3-4 viral particles of LNT-LXR-Nluc/eGFP per number of DECs seeded were resuspended in 1 ml of hepatic maturation 2 media with 5ug/ml of polybrene and slowly perfused with a 1 ml syringe through the 3-way connector connected to the catheter in the PV. The pump was restarted 30 min after the perfusion. For BALMs transduced with rAAV-LK03-CMV-eGFP, after 96h (day 25 of differentiation), the media in the bioreactor was discarded and rinse twice with PBS with the pump running at 1ml/min for 10 min. BALMs were either harvested at d25 or fresh hepatic maturation 2 media was added for another 2 days and harvested at day 27 of differentiation.
For BALMs transduced with LNT-LXR-Nluc/eGFP, after 48h (day 21 of differentiation), the media in the bioreactor was discarded and rinse twice with PBS with the pump running at 1ml/min for 10 min. Then fresh hepatic maturation 2 media with 1 µM T0901317 agonist was added for 96h and harvested at day 25 of differentiation. A minimum of 3 BALMs were transduced per viral vector.

Bioluminescence imaging.
BALMs transduced with LNT-LXR-Nluc/eGFP were dismantled from the bioreactor and perfused with 1 ml of NanoLuc luciferase substrate solution containing furimazine (20 µl substrate in 1 ml of PBS) (Nano-Glo ® Luciferase assay, Promega, UK) through the PV catheter. Imaging was performed on a cooled charge-coupled

device (CCD) camera (IVIS; PerkinElmer) for background reading and 5 min after addition of the substrate. Background values were subtracted to obtain corrected readings (at each time point/condition). Grey-scale photographs were acquired with a 12.5 cm field of view and then a bioluminescence image was obtained using a binning (resolution) factor of 4, a 1 f-stop, open filter and exposure time of 60 sec. Regions of interest (ROIs) were defined manually around each liver lobe. Signal intensities were calculated with Living Image software (Perkin Elmer) and expressed as Total Flux in photons per second.

NanoLuc Luciferase assay

Supernatants from PHHs or BALM media were stored at -20°C till analysis. 25 µl of sample was loaded on to a white 96 well plate, then 25 µl of NanoLuc luciferase reagent, was added using the luminometer's injector (Nano-Glo ® Luciferase assay, Promega, UK). The average of three readings per sample with an integration time of 1 sec was calculated. Luminescence was measured using a GloMax Navigator microplate luminometer with dual injectors (Promega, UK) and expressed as RLU/ml/h. For PHHs, the fold change was calculated between non transduced and transduced cells 48h after agonist activation. For BALMs, the fold change was calculated between the media harvested at d19 of differentiation (before transduction) and the media at d25 of differentiation (after agonist activation). The media of a BALM that was not transduced by any virus (BALM0) was used as a negative control. NanoLuc luciferase assay was performed on the media and measured with a GloMax luminometer (left); live imaging of BALMs was performed with an IVIS CCD camera, background readings were taken before perfusion of the substrate and total flux was calculated by substracting the background from the readings 5 min after substrate perfusion.

KEY RESOURCES TABLE

REAGENT or RESOURCE	SOURCE	IDENTIFIER
Antibodies		
Mouse monoclonal anti-Alpha-fetoprotein (AFP)	Sigma-Aldrich / Merck	Cat#A8452; RRID: AB_258392
Mouse monoclonal anti-Albumin (ALB)	Sigma-Aldrich / Merck	Cat#A6684; RRID: AB_258309
Mouse monoclonal anti-ASGR1 (ASGPR)	ThermoFisher scientific	Cat#MA1-40244; RRID:AB_2059674
Rabbit polyclonal anti-cleaved caspase 3 (CC3)	Cell Signalling Technologies	Cat#9661; RRID: AB_2341188
Mouse monoclonal anti-CD31	Thermofisher scientific	Cat# MA5-13188, RRID:AB_10982120
Mouse monoclonal anti-Cytokeratin 18 (CK-18)	Dako / Agilent	Cat#M7010; RRID: AB_2133299
Rabbit polyclonal anti-GFP	Abcam	Cat#ab290; batches GR3196305 and GR3270983-1;RRID: AB_303395
Rabbit polyclonal anti-HNF4α	Santa Cruz Biotechnology	Cat# sc-8987; RRID: AB_2116913
Rabbit polyclonal anti-Ki-67	Abcam	Cat#ab15580, RRID: AB_443209
Goat polyclonal anti-SOX-17	R&D Systems	Cat# AF1924; RRID: AB_35506
Bacterial and Virus Strains		
LNT-LXR-Nluc/eGFP	Dr. Juliette M. Delhove & Prof.T.McKay; ''This paper''.	NA
rAAV-LK03-CMV-eGFP	L. Lisowski; (Lisowski et al., 2014)	NA
Biological Samples		
Human long-term Hepatocytes in Monolayer (PHHs)	Biopredic International	Cat#HEP220, batch HEP2201007
Human umbilical vein endothelial cells (HUVECs), pooled donors screened for angiogenesis markers.	Lonza	Cat#C2519AS
Chemicals, Peptides, and Recombinant Proteins		
Albumin Peptide (ALB) FQNALLVR	GenScript; (Mazzacuva et al., 2019)	NA
Alpha-fetoprotein Peptide (AFP) TFQAITVTK	GenScript; ''this paper''	NA
Critical Commercial Assays		
Nano-Glo®Luciferase assay system	Promega	Cat#N1110
PrestoBlue® Cell Viability Reagent	ThermoFisher scientific	Cat#A13261
Experimental Models: Cell Lines		
hiPSC. Corrected A1ATD-hiPSC.	Prof.L.Vallier; (Yusa et al., 2011)	NA
HEK 293T viral producer cells	Dr. J.R.Counsell (Counsell et al., 2018)	NA
Experimental Models: Organisms/Strains		
Mouse: CD-1	Charles River	RRID:IMSR_CRL:022
Software and Algorithms		
Waters MassLynx V4.2	Waters, UK	NA
Leica Application Suite Advanced Fluorescence Lite 2.6.3 build 8173	Leica	NA
ImageJ 1.50d	(Schneider et al., 2012)	https://imagej.nih.gov/ij/
Other		
Selection of tryptic peptides for human albumin and human alpha-fetoprotein.	Global Proteome Machine MRM database	https://www.thegpm.org/

Supplemental References

Charrier, S., Ferrand, M., Zerbato, M., Precigout, G., Viornery, A., Bucher-Laurent, S., Benkhelifa-Ziyyat, S., Merten, O. W., Perea, J. & Galy, A. (2011). Quantification of lentiviral vector copy numbers in individual hematopoietic colony-forming cells shows vector dose-dependent effects on the frequency and level of transduction. Gene Ther, 18**,** 479-487.

Counsell, J. R., Karda, R., Diaz, J. A., Carey, L., Wiktorowicz, T., Buckley, S. M. K., Ameri, S., Ng, J., Baruteau, J., Almeida, F., et al. (2018). Foamy Virus Vectors Transduce Visceral Organs and Hippocampal Structures following In Vivo Delivery to Neonatal Mice. Mol Ther Nucleic Acids, 12**,** 626-634.

Cunningham, S. C., Dane, A. P., Spinoulas, A. & Alexander, I. E. (2008). Gene Delivery to the Juvenile Mouse Liver Using AAV2/8 Vectors. Molecular Therapy, 16**,** 1081-1088.

Grimm, D., Lee, J. S., Wang, L., Desai, T., Akache, B., Storm, T. A. & Kay, M. A. (2008). In vitro and in vivo gene therapy vector evolution via multispecies interbreeding and retargeting of adeno-associated viruses. J Virol, 82**,** 5887-5911.

Heywood, W. E., Camuzeaux, S., Doykov, I., Patel, N., Preece, R. L., Footitt, E., Cleary, M., Clayton, P., Grunewald, S., Abulhoul, L., et al. (2015). Proteomic Discovery and Development of a Multiplexed Targeted MRM-LC-MS/MS Assay for Urine Biomarkers of Extracellular Matrix Disruption in Mucopolysaccharidoses I, II, and VI. Anal Chem, 87**,** 12238-12244.

Mazzacuva, F., Lorvellec, M., Cilibrizzi, A., Mills, K., Heywood, W. E., Clayton, P. & Gissen, P. (2019). Mass Spectrometry Measurement of Albumin-Alpha Fetoprotein Ratio as an Indicator of iPSC-Derived Hepatocyte Differentiation. Methods Mol Biol, 1994**,** 149-156.

Schneider, C. A., Rasband, W. S. & Eliceiri, K. W. (2012). NIH Image to ImageJ: 25 years of image analysis. Nat Methods, 9**,** 671-675.

Sullivan, G. J., Hay, D. C., Park, I. H., Fletcher, J., Hannoun, Z., Payne, C. M., Dalgetty, D., Black, J. R., Ross, J. A., Samuel, K., et al. (2010). Generation of functional human hepatic endoderm from human induced pluripotent stem cells. Hepatology, 51**,** 329-335.

Vink, C. A., Counsell, J. R., Perocheau, D. P., Karda, R., Buckley, S. M. K., Brugman, M. H., Galla, M., Schambach, A., Mckay, T. R., Waddington, S. N., et al. (2017). Eliminating HIV-1 Packaging Sequences from Lentiviral Vector Proviruses Enhances Safety and Expedites Gene Transfer for Gene Therapy. Mol Ther, 25**,** 1790-1804.